Schweizerische Eidgenossenschaft
Confédération suisse
Confederazione Svizzera
Confederaziun svizra

Eidgenössisches Departement für Umwelt, Verkehr, Energie und Kommunikation UVEK

Bundesamt für Energie BFE
Sektion Cleantech

Final Report 28 02 2022

LeSoPot

Leveraging solar potential and waste heat utilization in buildings with a high temperature borehole thermal energy storage (BTES)

Datum: 28 02 2022

Ort: Dübendorf

Subventionsgeberin:
Schweizerische Eidgenossenschaft, handelnd durch das
Bundesamt für Energie BFE
Pilot-, Demonstrations- und Leuchtturmprogramm
CH-3003 Bern
www.bfe.admin.ch

Subventionsempfänger:
Empa, Urban Energy Systems Laboratory
Überlandstrasse 129, 8600 Dübendorf
www.empa.ch

Autoren:
Massimo Fiorentini, Urban Energy Systems Lab - Empa, massimo.fiorentini@empa.ch
Luca Baldini, Centre for Building Technologies and Processes - ZHAW, luca.baldini@zhaw.ch

BFE-Bereichsleitung:	Eckmanns Andreas, andreas.eckmanns@bfe.admin.ch
BFE-Programmleitung:	Stephan A. Mathez, stephan.a.mathez@solarcampus.ch
BFE-Vertragsnummer:	SI/501938-01

Bundesamt für Energie BFE
Mühlestrasse 4, CH-3063 Ittigen; Postadresse: CH-3003 Bern
Tel. +41 58 462 56 11 · Fax +41 58 463 25 00 · contact@bfe.admin.ch · www.bfe.admin.ch

Table of Contents

Abstract

In this study, a linearized modeling and optimization method for the design and control of energy systems with borehole energy storage (BTES) is presented, with the aim of exploiting the full potential of these storage systems in terms of seasonal smoothing of the electrical load profile and minimization of CO_2 emissions. In the study, it was shown that due to their seasonal variations, boundary conditions, such as the CO_2 intensity of the grid electricity or the availability of waste or solar heat, play an important role in the optimal design and operation of BTES with heat pumps. Achieving higher heat pump efficiency in winter while accepting lower efficiency in summer proves to be beneficial under certain conditions. The results show that a lower relative CO_2 intensity in summer than in winter leads to an overall higher optimal operating temperature of the BTES than typically used in the case of low-temperature BTES. This underscores that the use of high-temperature BTES storage systems (35-90°C) has untapped potential for CO_2 reduction, especially when energy sources with low CO_2 intensity in summer such as solar thermal, waste heat, or PV electricity are available.

In dieser Studie wird ein linearisiertes Modellierungs- und Optimierungsverfahren für die Auslegung und den Betrieb von Energiesystemen mit Erdsondenspeichern (BTES) vorgestellt, mit dem Ziel, das volle Potenzial dieser Speichersysteme im Hinblick auf die saisonale Glättung des elektrischen Lastprofils und die Minimierung der CO_2-Emissionen auszuschöpfen. In der Studie wurde gezeigt, dass Randbedingungen, wie die CO_2-Intensität des Netzstroms oder die Verfügbarkeit von Ab- oder Solarwärme, aufgrund ihrer saisonalen Schwankungen eine wichtige Rolle bei der optimalen Auslegung und dem Betrieb von BTES mit Wärmepumpen spielen. Das Erreichen einer höheren Wärmepumpeneffizienz im Winter bei gleichzeitiger Inkaufnahme einer geringeren Effizienz im Sommer erweist sich unter bestimmten Bedingungen als vorteilhaft. Die Ergebnisse zeigen, dass eine geringere relative CO_2-Intensität im Sommer als im Winter zu einer insgesamt höheren optimalen Betriebstemperatur des BTES führt, als dies bei Niedertemperatur-BTES typischerweise der Fall ist. Dies unterstreicht, dass der Einsatz von Hochtemperatur-BTES-Speichersystemen (35-90°C) ein ungenutztes Potenzial zur CO_2-Reduzierung bietet, insbesondere wenn Energiequellen mit geringer CO_2-Intensität im Sommer wie Solarthermie, Abwärme oder PV-Strom zur Verfügung stehen.

Cette étude présente une méthode de modélisation et d'optimisation linéarisée pour la conception et l'exploitation de systèmes énergétiques avec stockage par sondes géothermiques (BTES), dans le but d'exploiter pleinement le potentiel de ces systèmes de stockage en termes de lissage saisonnier du profil de charge électrique et de minimisation des émissions de CO_2. L'étude a montré que les conditions marginales, telles que l'intensité en CO_2 du courant de réseau ou la disponibilité de la chaleur résiduelle ou solaire, jouent un rôle important dans la conception et l'exploitation optimales des BTES avec pompes à chaleur en raison de leurs variations saisonnières. Dans certaines conditions, il est avantageux d'atteindre une meilleure efficacité des pompes à chaleur en hiver tout en acceptant une efficacité moindre en été. Les résultats montrent qu'une intensité relative de CO_2 plus faible en été qu'en hiver conduit à une température de fonctionnement optimale globale du BTES plus élevée que celle typiquement observée pour les BTES à basse température. Cela souligne le fait que l'utilisation de systèmes de stockage BTES à haute température (35-90°C) offre un potentiel inexploité de réduction des émissions de CO_2, en particulier lorsque des sources d'énergie à faible intensité de CO_2 sont disponibles en été, comme l'énergie solaire thermique, la chaleur résiduelle ou l'électricité photovoltaïque.

Project goals

The main objective of this project is to study the potential of a Borehole Thermal Energy Storage (BTES), designed with the intent to store thermal energy seasonally, in helping maximise the yearly performance of an energy system in terms of electric load profile shaving and CO_2 emissions.

The hypothesis is that the operating conditions of such storage, in particular its operating temperature, are a critical factor in determining its performance under defined system boundary conditions (yearly CO_2 emission profile of the electricity provider, heating and cooling demand profiles, supply and return temperatures for the supply network, etc.), and the integration of solar generation technologies can significantly vary the optimal configuration of the storage. It is thus expected that a higher BTES temperature would result when energy sources with low CO2 intensities in summer are available. This in turn would lead to a more significant seasonal load shift and thus higher heat pump performance in winter and therefore lower over-all CO2 emission.

In particular, it is envisioned that a replicable design and operation optimization methodology for energy systems with a BTES is developed in this project, modelling the dynamics of the system in a numerically tractable way to enable optimization algorithms to find the best system configuration while retaining the key physical phenomena that guarantee a good prediction performance compared to currently available modelling techniques.

Work carried out and results achieved

1. Background and literature review

A background and literature review of BTES implementations are presented in this section, aiming at providing the modelling methodology proposed in this study with the appropriate boundary conditions to be employed, common system configurations and BTES designs. The literature review was organized into two main sections, i) high temperature BTES systems and ii) low temperature BTES systems. High temperature BTES are typically employed in centralised solar-based systems or linked to a large industrial heat rejection source, and they can reach a maximum field temperature between 40° and 90°C. Low temperature BTES are generally designed to offer a wider integration of low temperature energy sources in newer generation district heating and cooling systems, and their maximum operating temperature is typically between 10° and 35°C.

1.1 High Temperature Systems

High temperature systems, which are generally built with a centralized solar system, have been studied for several years, but only a few full-scale implementations have been realized. These include systems built in Germany, Sweden, Denmark, Canada, Netherlands, Italy and China. A summary of the systems reviewed, with the publications used to extrapolate the key design and operational data, is reported inTable 1:

Table 1: Reference list for each BTES development

Country	Development	References
Denmark	Braedstrup	[1,2]
Italy	Treviglio	[3,4]
Sweden	Anneberg	[5–7]
Germany	Neckarsulm	[8,9]
Germany	Attenkirchen	[7,9–11]
Germany	Crailsheim	[3,10,12]
Netherlands	Groningen	[3,4,7]
Canada	Drake Landing	[7,13–15]
Sweden	Emmaboda	[16]
China	Chifeng	[17]

The careful analysis of these references, which includes reviews and studies relative to each specific implementation, allowed us to populate Table 2. In this table, we omitted the case studies of Treviglio, as not enough information could be retrieved to generate a meaningful analysis of this implementation, and Chifeng, as it is still a pilot of limited scale and it is difficult to be compared with the other BTES designs. This summary table includes design data relative to the BTES design and integration, as well as solar or waste heat generation, demand and distribution network, short term buffers and reported BTES efficiency and solar fraction of the system.

Table 2: Key design parameters of BTES implementations.

		Denmark Braedstrup	Germany Crailsheim	Germany Neckarsulm	Germany Attenkirchen	Canada Drake Landing	Sweden Emmaboda	Netherlands Groningen	Sweden Anneberg
Solar	Type		flat plate	flat plate	solar roof	flat plate		Evacuated Tube	flat plate
	H0 (MWh/m2)	1.025	1.13	1.15	1.17	1.381		1	1.07
	Field size (m2)	18600	7300	5500	800	2293		2400	2400
IWH / CHP			Y				Y		
Storage long	T min	16	20	15	15	45	40		30
	T max	50	65	65	90	65	60		45
	Size (m3)	19000	37500	63360	10500	34000	330000	23000	60000
	Depth (m)	45	55	30	30	35	150	20	65
	Aspect ratio	0.52	0.54	1.73	0.70	1.00	0.35	1.91	0.53
	Spacing (m)			2	2	3			3
	Soil thermal Cond. (W/m K)	1.42		2.2		2	3		4.1
	Borehole th. Resist. (K m/W)	0.172	0.5			0.6	0.02		0.045
	Vol. heat capacity (MJ/m3 K)	1.9		2.85	2.7	2.5*	2.2		2.2
	Tot capacitance (MWh/K)	10		50	8	24	202		37
	Tot heat capacity (MWh)	341		2508	591	472	4033	595	550
	N boreholes (strings X HE in string)	48 (16X6)	80	528	90	144 (16X6)	140	360	100 2*(10X5)
	Top insulation	0.5m mussel shells	0.4m foam glass	0.2m Poly-stirene	0.2m Poly-stirene				
Storage short	Type	Buffer tanks	Buffer Tanks	Distrib. tanks	Buffer tank	Buffer tank		Buffer tank	Distrib. Tanks
	Size (m3)		580	200	500	240		100	
Demand	Type	Residential	Residential	Mixed	Residential	Residential		Residential	Mixed
	Distrib T (supp)	80	75			55	50		60
	Distrib. T (ret)			43		37	35		20
	Extraction	HP	HP	HP	HP	Direct	Direct		Direct
	Energy (MWh/a)	4500	4100	1750	490	710		1162	550
Backup source	Heat Pump	Y	Y	Y	Y				
	El. Boiler								Y
	Gas Boiler	Y		Y		Y			
	Distributed								Y
Results	Solar Fraction	20%		39%	55%	97%		65%	40%
	Storage efficiency	63%	70%	41%	60%	36%		23%	46%
	Notes					*estimated		in 2nd year	

As one of the objectives of this study is to determine the possibility to shift the energy consumption from winter to summer, by charging the storage in summer with a heat pump when the CO_2 intensity of the grid is low (even if the COP is reduced), to then achieve a positive gain in winter, the dataset of Table 2 was divided into two main groups, i) systems with direct discharge, usually charged with only solar or waste heat, and ii) systems that use a heat pump to discharge the storage.

Some of the derived key indicators were plotted. In Figure 1a the higher and lower temperature operating limits of the BTES are plotted. Here it can be observed that all the systems that use a heat pump to discharge the storage have a generally similar or higher temperature boundary (between 50 and 65 °C) to the direct ones, but they can significantly reduce their lower temperature limit (30 to 45°C for the direct systems, 15-20°C for the heat-pump driven systems).

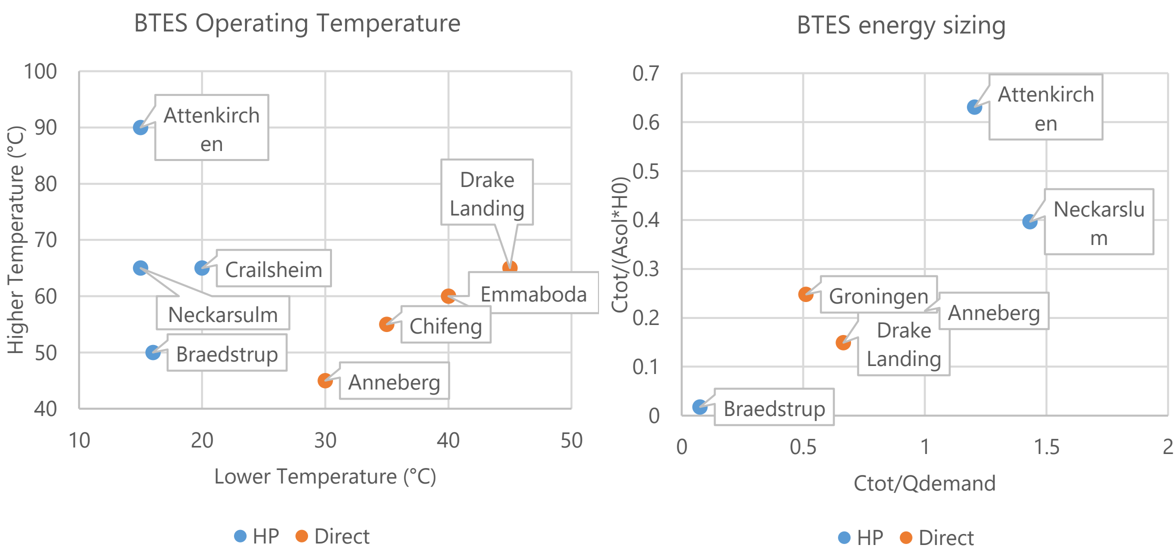

Figure 1: Surveyed BTES operating temperatures (left) and sizing of the BTES in respect to solar generation and district heating demand (right). Systems discharged with a heat pump are marked in blue, whether the ones directly discharged by the district heating network are marked in orange.

In Figure 1b, two indices indicative of the sizing of the BTES in comparison to the yearly potential solar generation and to the yearly district heating demand are plotted.

C_{tot}, the total heat capacity in MWh, was calculated by multiplying the total capacitance of the volume of ground in MWh/K by the expected temperature swing of the storage, as reported in Table 2. On the vertical axis of this figure the ratio between C_{tot} and the total yearly radiation multiplied by the area of the collectors is reported, whether on the horizontal axis C_{tot} is compared with the yearly demand. It is noticeable in the graph that all the direct systems implement a solar array which is significantly larger than the BTES total heat capacity, whether the BTES capacity is generally between half the value and the value of the yearly heating demand of the district. The heat pump-driven systems have a larger BTES capacity, but mostly because of the increased temperature difference in the yearly swing of 45-50°C compared to the 15-20°C of the direct systems.

The reported efficiency of the BTES, as it can be seen in Figure 2a, seem to be directly influenced by the aspect ratio of the system, where a larger diameter *D* compared to the depth *H* seem to have a negative impact on the efficiency of the BTES, with the best performing system being the ones with an aspect ratio of 0.5. It can also be noticed that the heat-pump driven system have higher reported efficiency in comparison to the direct systems with the same aspect ratio. This is due to reduced losses as the average yearly operating temperature can be reduced as a deeper discharge is enabled by the heat pump.

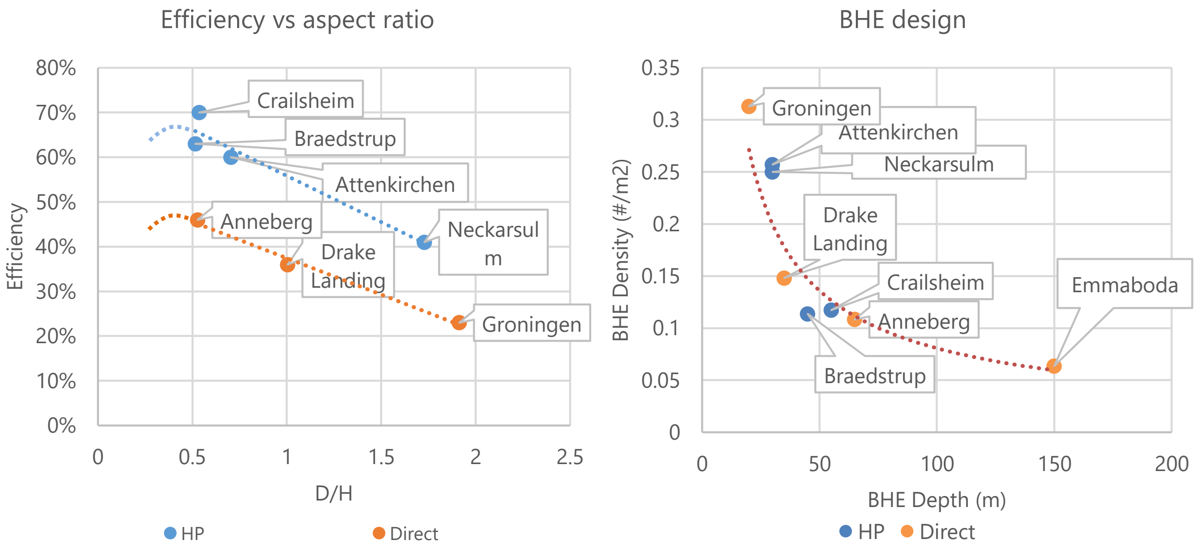

Figure 2: Surveyed BTES thermal efficiency vs their aspect ratio (left) and BTES density of boreholes vs their depth (right). Systems discharged with a heat pump are marked in blue, whether the ones directly discharged by the district heating network are marked in orange.

In Figure 2b, the distribution of the borehole depth and density (as number of boreholes per square meter) is plotted, showing that in general, shallower BTES installations have a higher density of boreholes per surface area. In Figure 3 the distribution of the reported network supply and return temperatures are shown, highlighting that heat pump-driven systems can operate a higher temperature supply network compared to directly driven systems, which are also strongly relying on low return temperatures to enable the discharge of the storage.

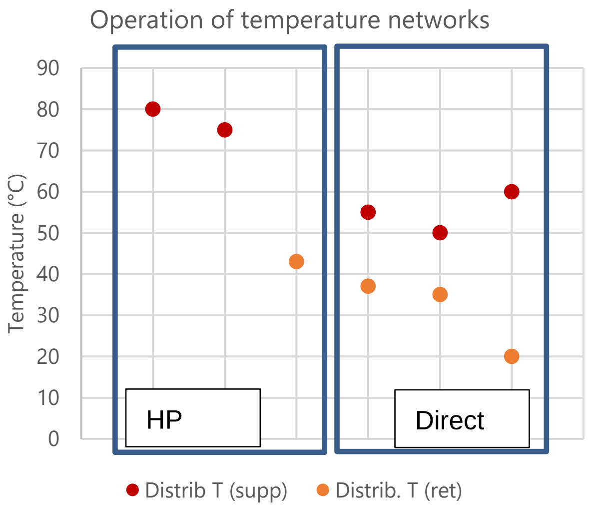

Figure 3: Surveyed BTES supply (red) and return (orange) networks operating temperatures.

1.2 Low Temperature Systems

Low temperature systems BTES systems are more variable in size and might not be centralized as higher temperature BTES. They are generally integrated into newer (5th generation) district networks and operate at low supply temperatures. As reported in the review conducted by Buffa *et al.* [18], Switzerland is one of the countries with most of these systems currently operational (see Figure 4). In this paper, a 5th generation district heating and cooling network are defined as "a thermal energy supply grid that uses water or brine as a carrier medium and hybrid substations with Water Source Heat Pumps (WSHP). It operates at temperatures so close to the ground that it is not suitable for direct heating purposes. The low temperature of the carrier medium allows exploiting directly industrial and urban excess heat and the use of renewable heat sources at low thermal exergy content. The possibility to reverse the operation of the customer substations permits to cover simultaneously and with the same pipelines both the heating and cooling demands of different buildings. Through hybrid substations, 5th generation district heating and cooling technology enhance sector coupling of thermal, electrical and gas grids in a decentralised smart energy system".

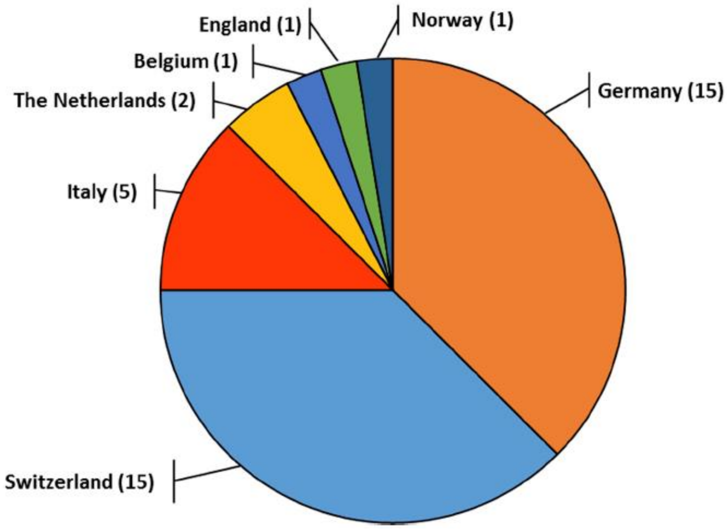

Figure 4: Geographical distribution of 5th generation district energy systems, as reported by Buffa *et al.* [18].

All the twelve low temperature BTES systems reviewed were recently built, mostly after 2012. The network supply temperature of BTES systems, compared to other 5th generation district energy systems, features a slightly larger temperature.

For example, the maximum variation in supply temperature of the systems in [18] was equal to 27°C, reported by the REKA village in Blatten-Belalp as can be seen from Figure 6 and Table 3. The higher network temperature could be due to the large cooling loads of the complex, which is a holiday village.

Table 3: Summary design data of 5th generation district systems integrating a low-temperature BTES [18]

Country	City	Year	Heat source	# of systems	# of bore-holes	Depth (m)	Tsupply,min (°C)	Tsupply,max (°C)
Germany	Biberach	2016	Ground	1	34	200	0	20
Germany	Herford	2000	Air/Ground	1	19	100	15	15
Germany	Schifferstadt	2017	Ground	1	28	100	12	12
Germany	Mainz	2011	Ground	1	4	300	8	9
Switzerland	ETH Campus	2013	Ground	3	431	200	8	24
Switzerland	FGZ Zurich	2014	Excess heat/ground	2	332	250	8	28
Switzerland	Suurstoffi	2012	other multisource	2	215 and 180	150 + 280	8	25
Switzerland	REKA village	2014	other multisource	1	31	150	8	35
Switzerland	"Sedrun" (Tujetsch)	2017	Air/Ground	1	73	250	8	8
Switzerland	Saas Fee	2015	Air/Ground	1	90	150	8	20
Switzerland	Richti Wallisellen	2014	Excess heat/ground	1	220	225	8	22
England	Derby	2012	Ground	1	28	100	6	10

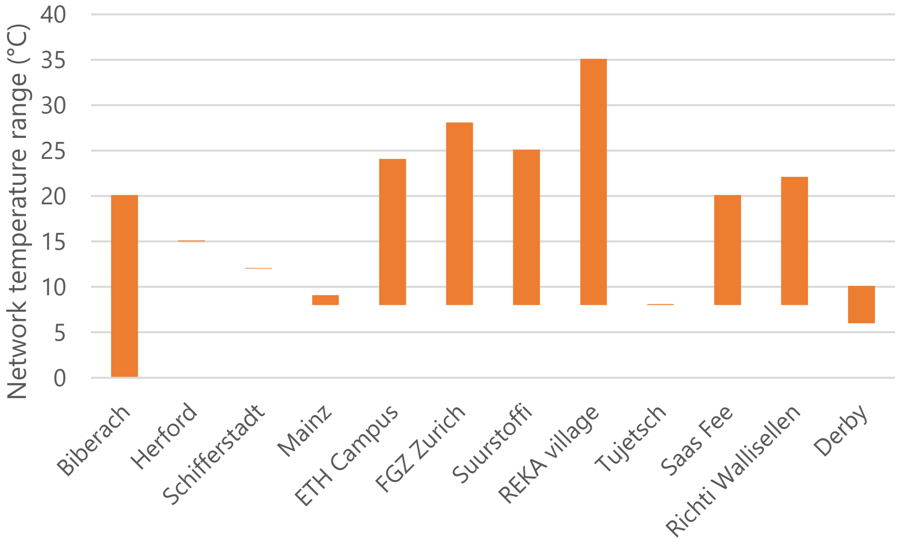

Figure 5: Supply network temperature variation in low temperature networks with BTES, as reported by Buffa *et al.* [18].

Differently from the high temperature systems, the low temperature 5th generation systems with a BTES have a single network that oscillates in temperature through the year, as shown in Figure 6, and the temperature is lifted or reduced for users by distributed heat pumps.

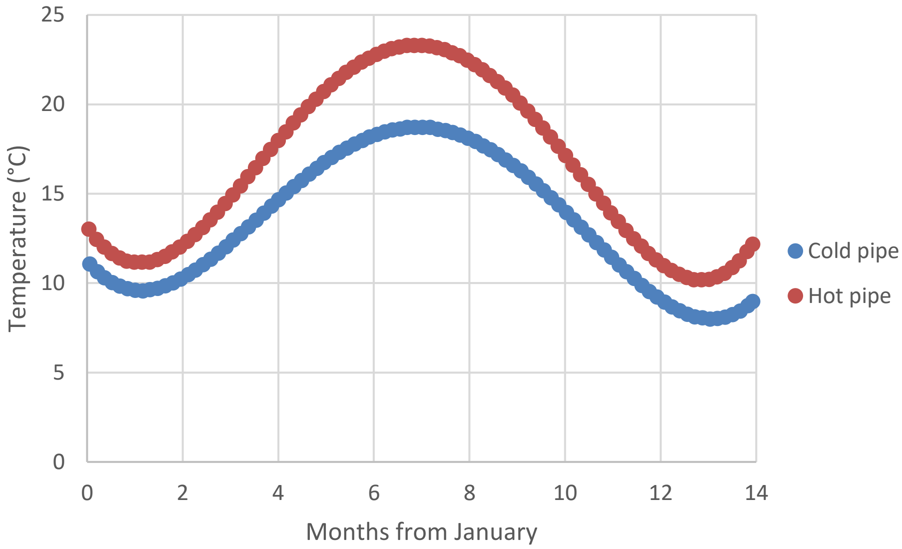

Figure 6: Average temperature oscillation in a low temperature network, data extracted from [19].

This low-temperature configuration allows easy integration of distributed thermal prosumers on the network, and reduces the thermal losses on the network and storage. On the other side, compared to higher temperature networks, the low ΔT between supply and return pipes leads to larger pipe diameter and storage thermal capacity, and the pumping costs per unit of energy are higher due to small operative ΔT and higher fluid viscosity [18].

1.3 Energy system components and system configurations

The BTES has a central role in this study, and several system components play a key role in supporting its operation over the course of the year. The most relevant components include additional renewable thermal generation, or industrial waste heat, short term buffer storage, energy conversion devices (e.g. heat pumps/chillers, gas boilers) and distribution infrastructure.

1.3.1 Thermal Generation

Assuming the BTES is integrated into a district heating and cooling system, as Switzerland has a heating-dominated climate, the waste heat recovery from the cooling operations alone it is expected to be generally not sufficient in covering the entire yearly heating demand. For this reason, solar thermal generation is included in the design optimization methodology for the BTES and its supporting systems. The reviewed high temperature BTES systems always feature a high temperature source, mostly from solar flat-plate (90% [7]) or evacuated tubes, and it is generally the only energy source for charging the seasonal storage. The area covered by the solar panels in these implementations is presented in Table 2, and its relative size compared to the total heat capacity of the BTES is presented in Figure 1. Low temperature BTES in 4th and 5th generation networks, as they operate at lower temperature, accept also lower temperature waste heat, from collectors that generate heat at lower temperatures, such as photovoltaic-thermal panels (PVT). Examples are provided by the Swiss district energy system of the REKA village [20] and Suurstoffi [21,22]. While solar is one source of regeneration of the storage, it is not always employed when other sufficient sources are present, such as industrial waste heat.

1.3.2 Short-term thermal storage

Short-term thermal storage devices, which from a district system design perspective can support the matching between generation and demand from short-timeframe fluctuations, are important for the BTES operation as well. They are particularly effective in ensuring that all the heat available to be transferred to/from the BTES gets actually transferred. BTES systems can store large amounts of heat, but they generally have a relatively low heat transfer rate. This affects their possibility to accept a high variability in available heat to be charged, or cover a fluctuating demand that exceeds the power capabilities of the borehole field. All the reviewed high-temperature systems have short-term buffer tanks to smoothen the day-night energy flux variation, but they vary significantly in terms of design, as reported in Table 2. They can be centralized or distributed, depending on the system layout and operation. The key design parameter for this type of buffer analyzed in this study is the size of the tank for the solar generation.

1.3.3 Energy conversion devices and system layout

The reviewed high temperature systems were classified into two main categories, direct or heat-pump driven systems. High temperature systems, especially direct systems, use gas or electric heaters mainly as a backup source, to add on an insufficient energy output from the BTES. Indirect systems, which utilise a heat pump to discharge the BTES, enable a deeper discharge of the BTES and allow a higher degree of control on the supply side, whether in direct systems the BTES require a sufficiently high temperature for discharge in comparison to the return temperature from the district network. The schematic layout of each system was derived to visualize the connections of the key system's components. The schematic of two successful systems, one direct (Drake Landing) and one heat pump-driven (Crailsheim) are presented in Figure 7.

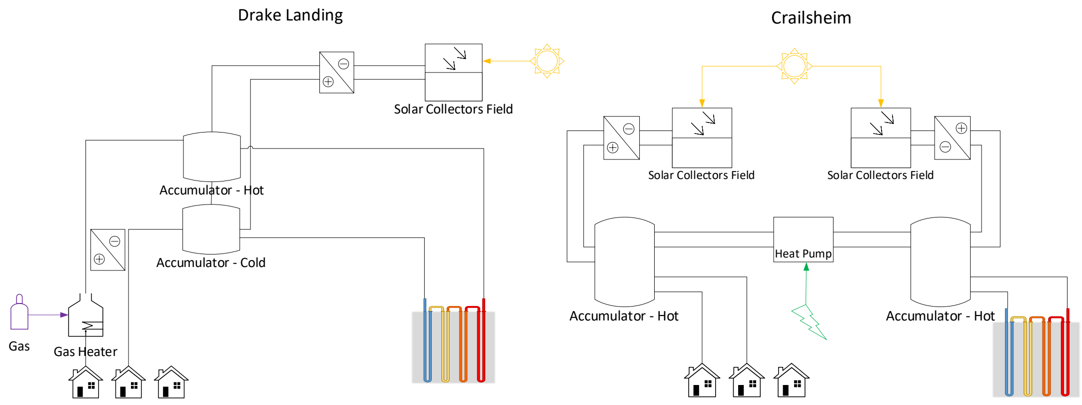

Figure 7: Schematic layouts of Drake Landing and Crailsheim.

When low-temperature BTES systems are implemented, the network is designed for having heat pumps to lift the temperature for the decentralized users, which can also contribute to the charging of the storage, or integrate on the low temperature side of the system generators at lower temperatures (example in Figure 8).

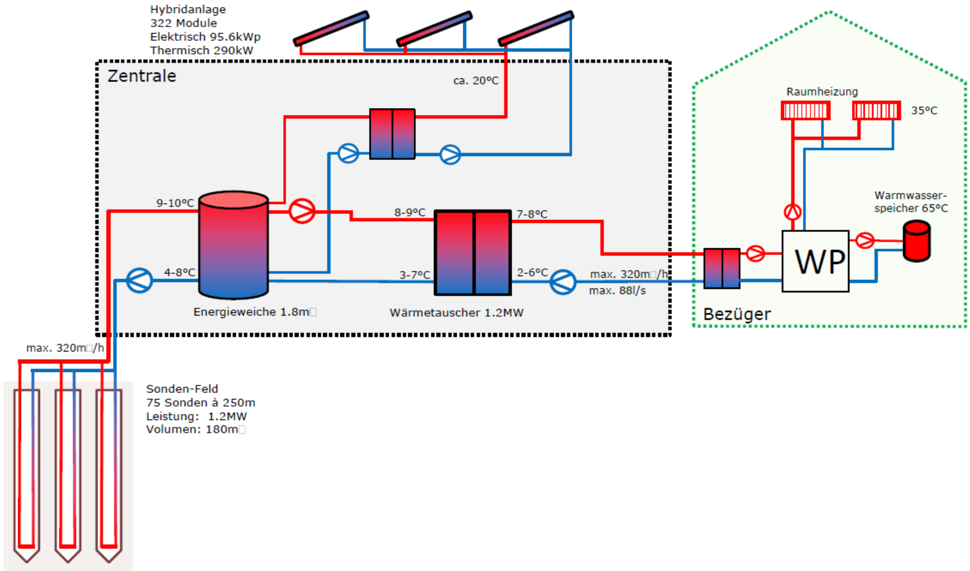

Figure 8: Schematic of the energy system of the REKA village, as presented in [23].

With the idea of integrating not only low-temperature thermal energy sources, but also excess renewable electrical generation, this study focused on heat-pump driven BTES systems, that can eventually be operationally used directly if is this a more efficient solution under certain conditions. Technologies that use fossil fuels, such as gas burners, are not included in this study.

1.4 Research questions and definition of testing methodology

One of the key hypotheses to be tested is if and under which operating conditions a BTES system is most effective in seasonally storing the waste heat generated by a heat pump in the cooling operations in summer, when the CO_2 emissions intensities are low, to reduce the electrical energy consumption of the heat pump in heating operations in winter, when the CO_2 emissions intensities are high.

The design and operation optimization methodology developed in this study, that enables answering the aforementioned and other similar research questions, needs to be generalizable and able to assess the optimal design and operating sequences of different systems under various boundary conditions.

Several models have been built to determine the performance of a BTES system, accounting for both, the large-scale heat flow in the ground volume and the local processes in the borehole. The report made by Sintef [24] provides a comprehensive review of the currently available simulation models available and implemented in commercially available software. Most of these models are not control/optimization oriented, which are in general linearized to allow their computational optimization for design and operation needs. For this reason, one of the objectives of this research was to develop a linearized modelling methodology, particularly for control and design optimization purposes, and implement them in relevant optimization frameworks.

Control optimization: The first research question is on the control of the BTES, and the necessity to determine the best-operating conditions for a heat pump-driven BTES, subject to different yearly CO2 intensity profiles of electricity supply. To enable this numerical optimization, a control-oriented model is required, with the capability to describe the effects on the electric load of the heat pump and circulation system of parameters including the BTES plumbing configuration (in-series or in-parallel or mixed — allowing mode switching), supply temperature and flow rate to the BTES. For this purpose, this study proposes a linearized modelling method for the storage temperature dynamics, based on a resistance–capacitance (R–C) equivalence and linearized heat transfer calculation within the boreholes, which is then calibrated and validated against a high-fidelity TRNSYS model. This model, differently from other modelling techniques available in the literature, allows for the estimation of the thermal response of the ground with dynamically changing inlet temperatures, flow rates and plumbing configurations, in conjunction with the expected consumption for the circulation of the HTF. Coupling this model with a linearized expression for the inverse of the heat pump's COP, a bilinear optimization problem is obtained, which enables the possibility to find an optimal open-loop solution for a system under defined boundary conditions. This methodology, summarized in this report in Section 2, is presented in more detail in [25].

Design optimization: Current design optimization approaches employ significantly simplified models (e.g. a storage capacity with constant losses) to enable the application of numerical optimization methods to determine the best seasonal storage and supporting equipment capacity. Nevertheless, the optimal size of the seasonal thermal energy storage and its operational conditions (e.g. temperature evolution) are linked. The storage operating conditions also affect the efficiency of the equipment connected to it. This paper, therefore, proposes a non-convex optimization programming formulation that, differently from the studies available in the literature, can consider:

• The influence of operational decisions such as the initial temperature of the BTES storage temperature swing on the total capacity of the storage and thermal losses of the storage.

• The connection between the volume of the BTES storage and its maximum heat transfer rate.

• The effect of the temperature difference between heat transfer fluid (HTF) and storage on the heat transfer rate when the storage is charged or discharged and as well as on the efficiency of the connected heat pump or chiller.

• The impact of boundary conditions such as the availability of solar thermal generation, the CO_2 intensity of the grid electricity consumed, the ratio between heating and cooling (rejected waste heat) demand, and price of direct CO_2 emissions.

This methodology, summarized in this report in Section 3, is presented in more detail in [26].

2. BTES operation optimization

2.1 BTES High-detail modelling

As the objective of this study is to optimize the performance of a BTES, it is necessary to develop a control/optimization-oriented model of the storage to be able to numerically solve the problem. To achieve this accurately, a benchmark platform for the evaluation of the performance of the BTES and of the reduced-complexity model is necessary. For an accurate description of the BTES thermal behaviour, TRNSYS 18.02 was chosen as the preferred simulation software. An unreleased TRNSYS Type based on the TRNSBM developed by Pahud [27] was used, as this Type allows for different hydraulic connections between the boreholes and offers the flexibility needed for performance optimisation. The theoretical foundation of the simulation model the superposition method is introduced by Eskilson in [28].

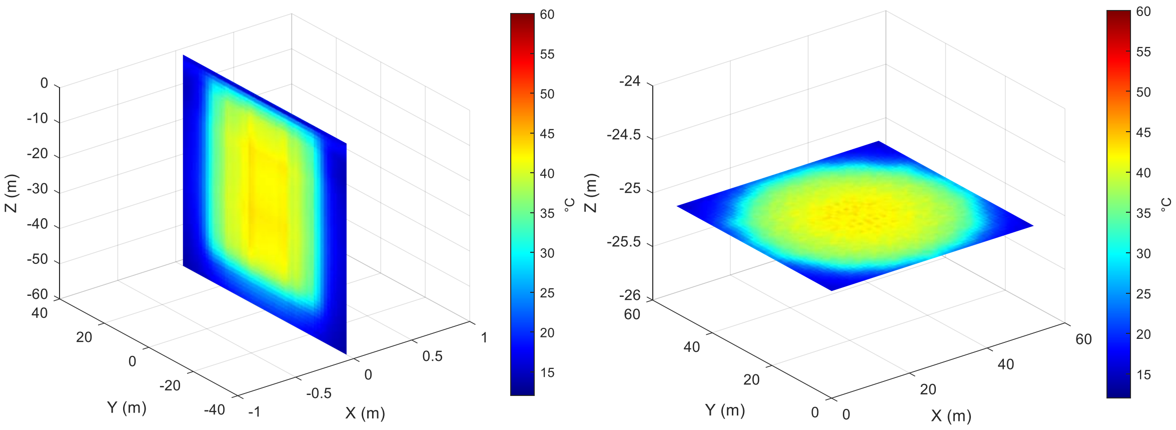

Figure 9: Temperature distribution of the BTES volume at week 228, using Empa campus demand data, TRNSYS simulation in-series configuration, a) vertical plane cut and b) horizontal plane cut at 25m depth.

The Superposition Borehole Model (SBM) used in this TRNSYS type is a detailed and validated finite-difference model that allows the evaluation of a BTES in an arbitrary configuration, which, while not suitable for optimization purposes, can be used as a reference for a control-oriented model. Optimizing the charging and discharging conditions of the BTES is critical to ensure that the maximum amount of heat available to be stored is transferred to the ground and effectively extracted later in the year, using the least amount of electrical energy as possible to generate the heat with a heat pump and move the water into the BHEs. The BTES case-study field, designed for the Empa campus, is of cylindrical shape with a diameter of approximately 51m. It includes 144 double-U ground heat exchangers (GHXs), 50 meters deep, and with a layer of insulation above the borehole field. The construction details of the BTES and the heat exchangers are summarized in Table 4, and based on the design presented by Weber and Baldini for the Empa campus[29]. For simplicity, the ground is assumed to be at a constant initial temperature and without an initial depth-related temperature gradient. The BTES can be connected either with 18 in-parallel circuits with 8 GHXs in-series, or all the GHXs in parallel.

Table 4: Case study BTES construction details

Parameter	Value
Borehole diameter (m)	0.14
U-pipe outer diameter (m)	0.04
U-pipe thickness (m)	0.0032
U-pipe thermal conductivity (W/m K)	0.35
U-pipe shank spacing (m)	0.06
U-pipe starting depth (m)	1
U-pipe length (m)	50
Filling thermal cond. (W/m K)	0.6
Contact resistance pipe/filling (m K/W)	0.02
Heat conductivity ground layer (W/m K)	2.4
Volumetric heat capacity ground layer (kJ/K m^3)	2200
Heat transfer coefficient air to ground (W/m^2 K)	0.08
Initial ground temperature (°C)	12

The in-parallel and in-series connections of the BHXs, as presented in [29], are shown in Figure 10.

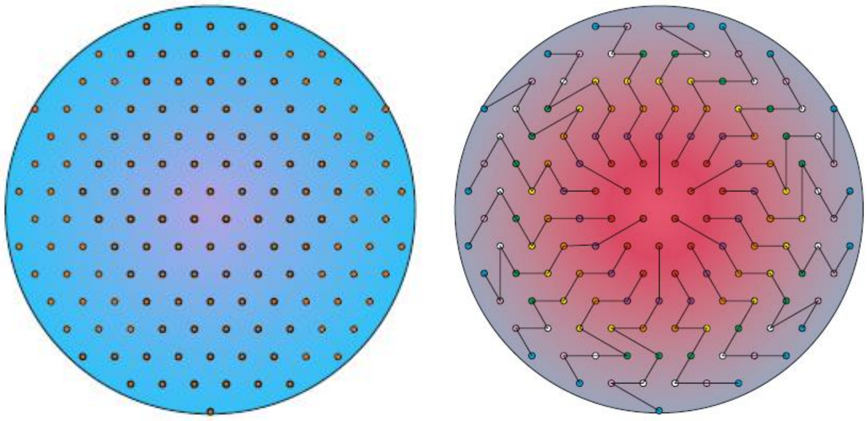

Figure 10: BTES case study, in-parallel and in-series plumbing configurations

2.2 Control-oriented modelling of the BTES

As the modelling needs to be used for design and operation optimization purposes, a linearized approach was taken to describe the heat transfer in the ground and through the borehole heat exchangers.

In particular, under the assumptions that i) the boreholes are evenly distributed, ii) the borehole has a cylindrical shape and iii) only sensible heat processes are described, a Resistance – Capacitance (R-C) equivalent for the heat conduction in the ground could be used.

Under these assumptions, the volume of the storage could be divided into a number of slices, equal to the number of parallel channels of the plumbing configuration. Each slice of the cylinder can be then divided into a number of sections, equal to the number of in-series connections of the configuration, as presented in Figure 11.

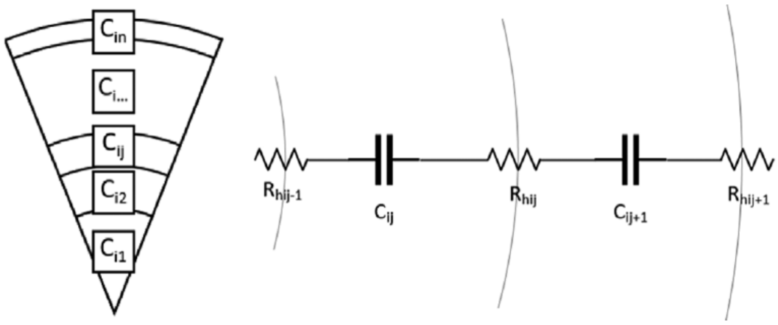

Figure 11: Resistances and capacitances in a section of the BTES cylinder.

A network of vertical and horizontal resistances, linking sections of ground represented by lumped capacitances, was built. An example of this R-C network can be seen in Figure 12.

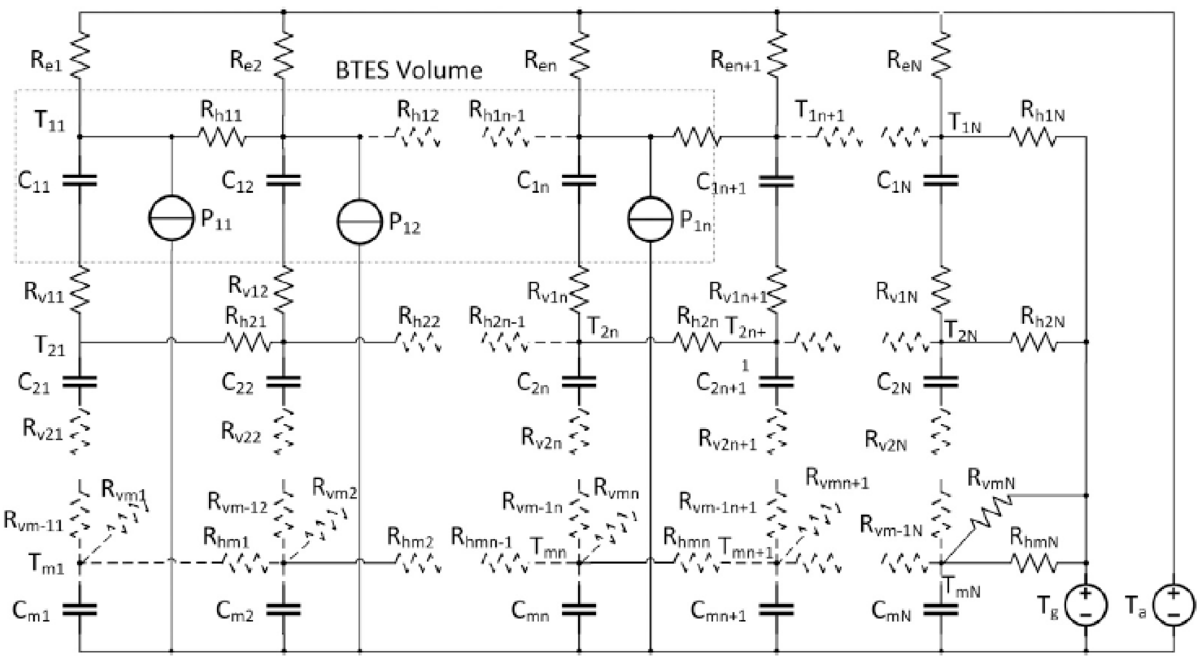

Figure 12: R-C Network of the ground cylinder slice.

The heat exchange occurring in the boreholes, under the assumption that each borehole is exposed to a constant temperature boundary, equal to the temperature of the capacitance that it is forcing, has a non-linear relationship (Logarithmic Mean Temperature Difference). To enable the possibility to perform on- and off-line optimization, the heat generation within the boreholes, which in this diagram is represented by the heat generators $P_{11},\ldots,P_{1n}$, was also linearized, utilizing the Arithmetic Mean Temperature Difference instead of the logarithmic one. This approach, that reduces the heat exchange to the one of a single pipe exposed to a constant temperature, would over-estimate the heat exchange to the ground, as the thermal connection between the downwards flowing section of the pipe and the upwards flowing one (as described in detail in the modelling proposed in [30]) is neglected. Therefore, a lumped "identifiable" resistance of the borehole is included in the estimation of the total heat exchange coefficient of this equivalent pipe. This lumped resistance includes the borehole filling, pipe material and contact conduction resistances, and adds to the forced convection heat exchange one.

The value of this identifiable resistance is found by minimizing the root-mean-square error (RMSE) between the predicted power delivery of the BTES and the more accurate one calculated via the more time-consuming TRNSYS simulation. A comparison of the modelled heat-transfer with the linearized approach in comparison to the one calculated using TRNSYS with the same mass flow and temperature inputs is presented in Figure 13.

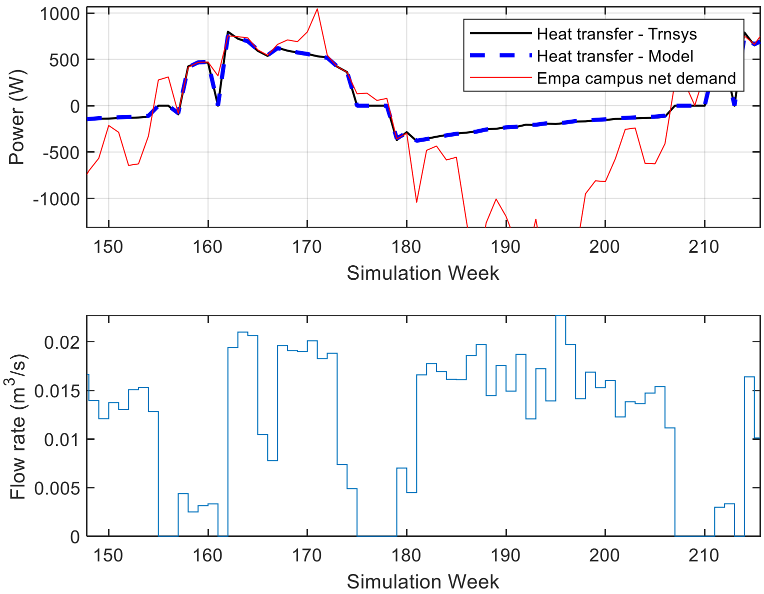

Figure 13: Comparison between heat transfer calculation between proposed linearized modelling and TRNSYS.

The validation was also performed on the thermal response of the ground, at different distances from the centre of the cylinder. This was done by dividing the BTES cylinder into 8 concentrically delimited volumes of equal capacitance (as many as the in-series connections), and a comparison of the temperature profile in these volumes from the TRNSYS results and from the proposed Matlab model are shown in Figure 14.

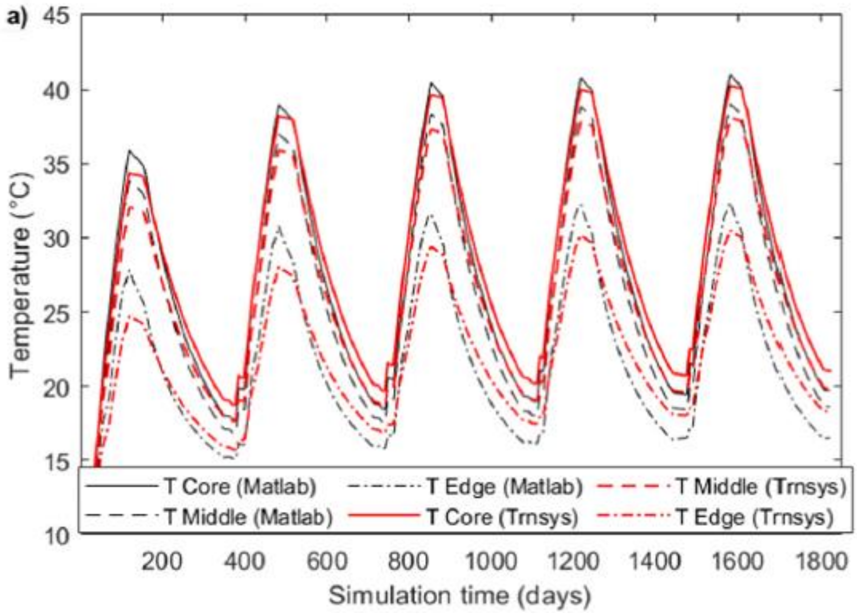

Figure 14: Comparison of thermal response of the ground between TRNSYS proposed Matlab model. Temperature at the BTES core, middle and periphery (edge) are presented for a 5 year simulation, in-series configuration.

2.3 Operation optimization framework

The linearized BTES model, as presented in Figure 12: R-C Network of the ground cylinder slice. Figure 12 can be used to optimize the operation of the system over a defined horizon, for planning and real-time control purposes. As the system is defined by discrete and continuous variables, the optimization results in a mixed integer programming (MIP) problem. The total heat absorbed or released by the BTES unit, Pth, is calculate from the model's output array.

A number of constraints were included in the optimization framework, such as that i) The system can only operate in one of the possible q modes or at one pump speed at a time, ii) The supply temperature to the storage is also limited by constraints on the physical limits of the heat pump, and should be higher than the core of the storage volume if the BTES is being charged, and lower than the edge of storage volume if it is being discharged and iii) the heat transferred to and from the BTES must be lower than the available heat to be charged or the requested one to be discharged.

With the model and these constraints in place, a cost function was then used to minimize the yearly CO_2 emissions of the system, as described in Eq. 1:

$$J = \sum_{k=1}^{N} (I_{CO_2}(k) P_{el,rem}(k) + I_{CO_2}(k) P_{el}(k) + \sum_{p} I_{CO_2}(k) R(p) u_d(q,k)) \tag{1}$$

Where I_{CO2} is the CO_2 intensity of the electricity from the grid at each time step k, R(p) is the electrical consumption of the circulation pump in each operating mode and P_{el} and $P_{el,rem}$, are the electricity consumption of the heat pump to transfer the heat P_{th} to/from the BTES at a defined inlet temperature and the heat pump electricity consumption to meet the remainder of the demand of the system respectively.

The control-oriented modelling of the BTES and the optimization was undertaken using Matlab as a platform, Yalmip [31] as a toolbox for optimization and Gurobi v9.1 [32] as a solver suitable for the bilinear mixed-integer model of the BTES and heat pump developed in this study.

2.4 Empa case study results

The Empa campus is located in Dübendorf and includes 35 buildings of different use (e.g. office, laboratory, etc.). The Empa campus requires both heating and cooling throughout the year due to various building types, and the thermal energy, currently generated with a natural gas boiler and a chiller, is distributed to the buildings using three networks at different temperatures, as presented in the study by Weber and Baldini [29]. For this study, the network has been simplified by removing the gas heater and assuming a heat pump with infinite capacity can supply the required demand for heating and cooling throughout the year. The system schematic is presented in Figure 15. It should be noted that in this priniple schematic valves are placed to ensure the required operating modes are feasible and unintended flows are avoided.

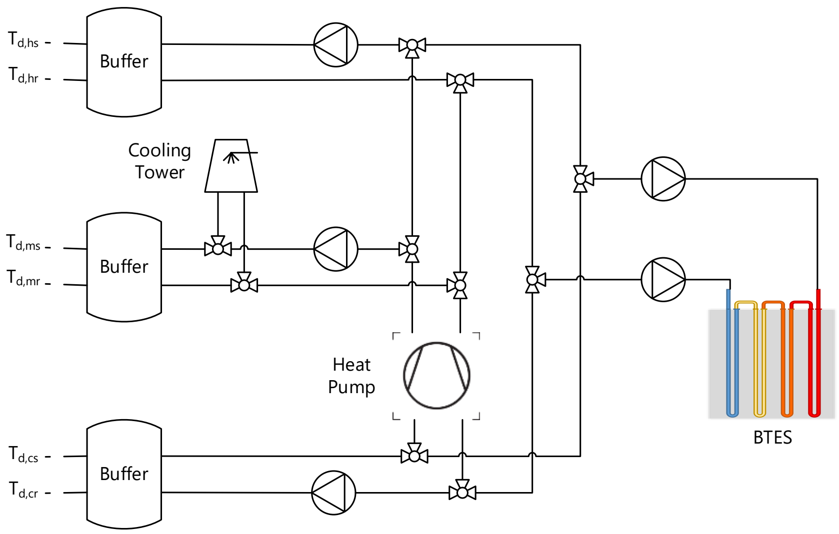

Figure 15: Principle schematic of integration of the BTES in the Empa campus heating and cooling network.

The high temperature network supplies heat at 65°C ($T_{d,hs}$) and has a return of 45°C ($T_{d,hr}$). The mid-temperature network is used for both low-temperature heating and heat rejection, operates between 38 ($T_{d,ms}$) and 28°C ($T_{d,mr}$). The cooling network supplies cold water at 6°C ($T_{d,cs}$) and has a design return temperature of 12°C ($T_{d,cr}$). It was assumed that, when the heat could not be exchanged with the BTES, in cooling operation it would be rejected at 35°C and in heating operation at 1°C. The heat pump was assumed to operate with a COP as expressed in Eq. 2:

$$COP = 0.6\left(\frac{T_h}{T_h - T_c}\right) \tag{2}$$

A reference CO_2 intensity profile of the Swiss grid was sourced from ElectricityMap [33]. To generate a profile with lower intensity in summer (mimicking for example the introduction of additional solar energy), the same profile was then modified reducing the intensity in summer by 2/3. The two profiles are presented in Figure 16, where the week 0, the beginning of the simulations, was considered to be the week of the 15th of May, as the demand shifts towards cooling and the charging of the BTES begins.

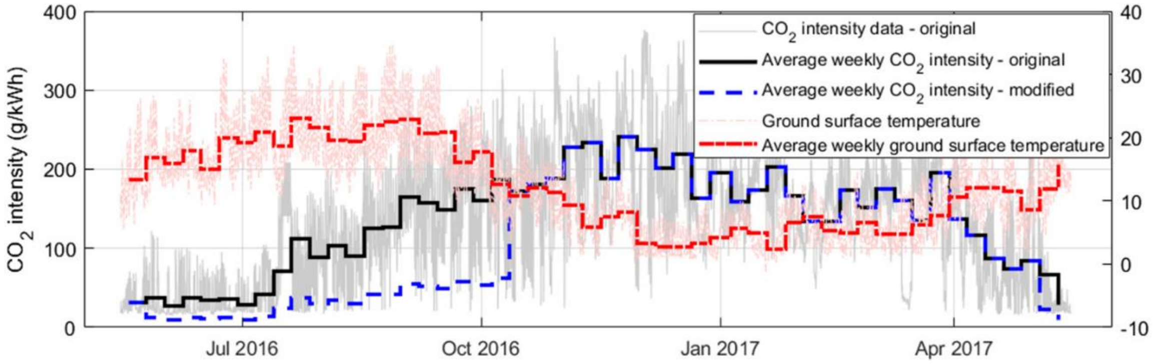

Figure 16: Standard and modified CO_2 profiles.

The measured net demand for heating and cooling of the Empa campus was used as an input to the calculations (Figure 17).

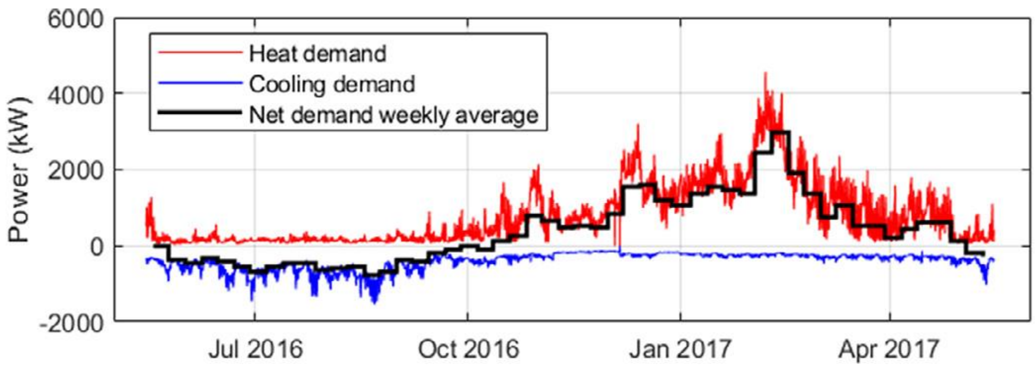

Figure 17: Empa campus measured heating and cooling demand profiles.

The operation of the BTES was tested for each plumbing configuration (in-series and in-parallel) and employing four control approaches: three baseline controllers with constant charging/discharging temperatures and variable flow rate, and one optimized controller with variable charging and discharging temperatures). In addition, a controller with the possibility to operate in ‘‘mixed-mode’’, where the plumbing configuration could be dynamically changed from parallel to in-series and vice versa, was also considered (see [25] for a more detailed description of the control approaches). A scenario where no BTES is integrated into the energy system, where all the heat is rejected and sourced at the aforementioned fixed temperatures, was also considered as a reference.

A summary of all the 9 control scenarios analysed in this study, together with the scenario without a BTES, is presented in Table 5. These control scenarios were tested in both CO_2 intensity profile cases.

Table 5: Simulation scenarios summary description.

Scenario	Description	Charging Temp.	Disch. Temp.	Pump speed
No BTES	No BTES integrated in the energy system	-	-	-
Base Series 65/12	Baseline control, in-series config.	65°C	12°C	Variable
Base Series 65/20	Baseline control, in-series config.	65°C	20°C	Variable
Base Series 35/12	Baseline control, in-series config.	35°C	12°C	Variable
Base Parall. 65/12	Baseline control, in-parallel config.	65°C	12°C	Variable
Base Parall. 65/20	Baseline control, in-parallel config.	65°C	20°C	Variable
Base Parall. 35/12	Baseline control, in-parallel config.	35°C	12°C	Variable
Optimal Series	Optimal control, in-series config.	Var. ≤ 65 °C	Var. ≥ 12°C	2 fixed
Optimal Parall.	Optimal control, in-parallel config.	Var. ≤ 65 °C	Var. ≥ 12°C	2 fixed
Optimal Mixed	Optimal control, mixed-mode conf.	Var. ≤ 65 °C	Var. ≥ 12°C	1 fixed per mode

2.4.1 Results and discussion

The results from these simulations highlight that the CO_2 intensity profile is crucially important in determining the best BTES operation strategy. Observing in Figure 18 the total CO_2 emission obtained using the standard CO_2 emission intensity profile it can be noticed that, between scenarios employing a baseline control, the low-temperature ones (35/12) achieve the best performance, with the in-series and in-parallel configuration obtaining similar results. It can also be noticed that a high-temperature BTES is not beneficial in this CO_2 intensity profile case, even in comparison to the case without a BTES storage: the reduction of CO_2 intensity in summer is not sufficient to compensate for the higher energy consumption of the baseline operating at higher charging temperature (65/12 and 65/20), as shown in Table 6.

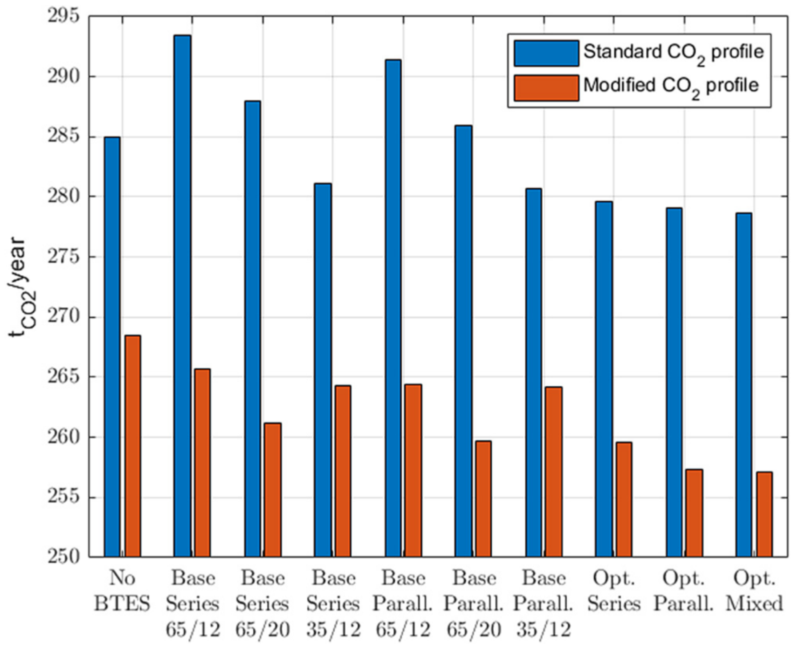

Figure 18: Yearly CO_2 emission in the various scenarios.

The low-temperature baseline controllers used less electrical energy compared to the scenario without a BTES (Table 6). This is to be expected as the baseline controllers charge the BTES at the same temperature as the heat pump would reject the waste heat when cooling, allowing the system to reclaim some of this heat during winter. Similarly, the optimal controllers used less electrical energy.

Table 6: Yearly CO_2 and electrical energy results comparison between baseline and optimal controllers, standard (std) and modified (mod) CO_2 profiles. Worst and best-performing baseline controllers in each CO_2 profile scenario highlighted in light red and green respectively, best-performing controllers highlighted in dark green.

	CO2 (std) (t_{CO_2}/y)	CO2 (std) diff.	CO2 (mod) (t_{CO_2}/y)	CO2 (mod) diff.	El. Energy (MWh/y)	El. Energy diff.
No BTES	285.0	0%	268.5	0%	1836.1	0%
B. Series 65/12	293.5	3.0%	265.7	-1.0%	1992.6	8.6%
B. Series 65/20	288.0	1.1%	261.1	-2.7%	1957.1	6.6%
B. Series 35/15	281.1	-1.4%	264.3	-1.6%	1818.6	-1.0%
B. Par. 65/12	291.4	2.2%	264.4	-1.5%	1969.0	7.2%
B. Par. 65/20	286.0	0.3%	259.7	-3.3%	1940.2	5.7%
B. Par. 35/15	280.7	-1.5%	264.1	-1.6%	1814.4	-1.2%
Opt Ser (std)	279.6	-1.9%			1810.2	-1.4%
Opt Par (std)	279.1	-2.1%			1812.7	-1.3%
Opt Mix (std)	278.7	-2.2%			1808.1	-1.5%
Opt Ser (mod)			259.6	-3.3%	1868.9	1.8%
Opt Par (mod)			257.3	-4.2%	1910.7	4.1%
Opt Mix (mod)			257.1	-4.3%	1900.6	3.5%

An example of the evolution of the BTES temperature when the optimal controllers were employed, compared to the baseline low- and high-temperature ones, is shown in Figure 19, where the results for the in-parallel configuration is presented.

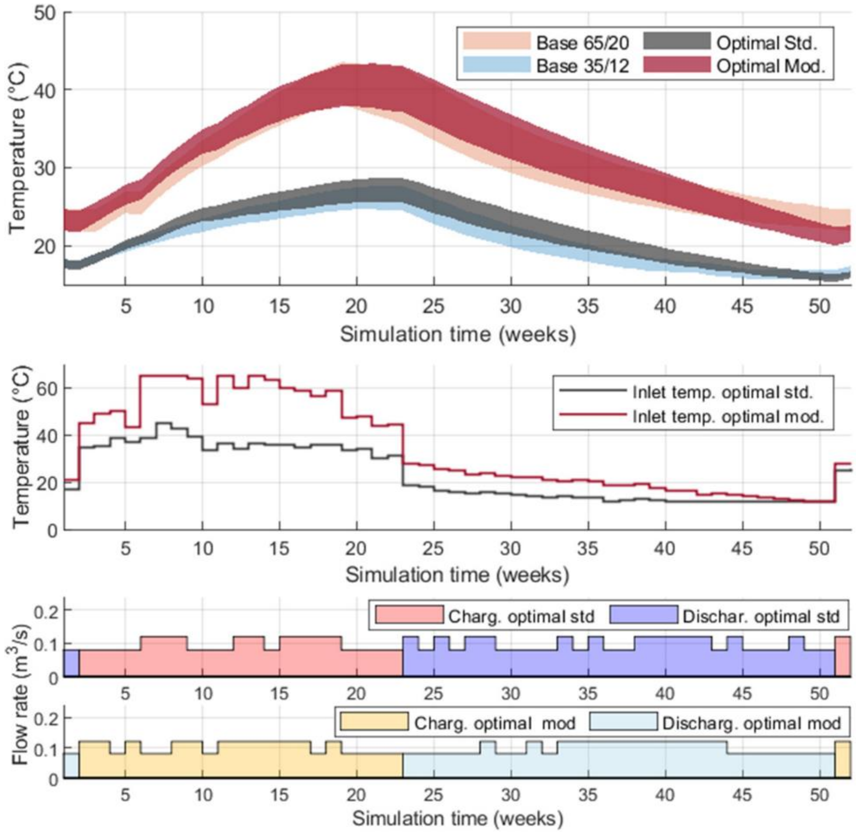

Figure 19: BTES temperature range (above) of the baseline controllers and optimal ones (with standard and modified CO_2 profile) employing the in-parallel configuration; and (below) supply temperature profile and flow rate management of the optimal controllers.

In the standard CO_2 case the optimal controller behaved again similarly to the Baseline 35/12 scenario, but with a slightly higher temperature swing, as a result of a slightly higher inlet temperature throughout the charging phase. In the modified CO_2 intensity profile case, the optimal controller followed again a similar trend to the Baseline 65/20 scenario, but in this case, reaching a similar peak temperature. This was also achieved, in the charging phase, by increasing the supply temperature increasing to 65°C after the first 6 weeks, but remaining relatively higher in comparison to the in-series configuration for the remainder of the charging phase. A similar linear decay of the inlet temperature was noticeable in the discharging phase results, but more pronounced, from 28°C to 12°C.

As a generally low reduction in CO_2 emissions was reported in these results, mostly due to the unbalanced heating and cooling yearly demand and limited size BTES, a further calculation was undertaken to estimate the potential reduction in CO_2 emission from a BTES appropriately sized for a more balanced heating and cooling demand, or the addition of an external heat source during summer. To this end, the CO_2 emissions of only the heating and cooling provided by the BTES in each optimal control scenario were calculated, and compared to the emissions of the same heating and cooling demand profiles provided by the base system without a BTES. An example of the charging and discharging operations considered is provided in Figure 20, where the optimal in-parallel controller case is presented.

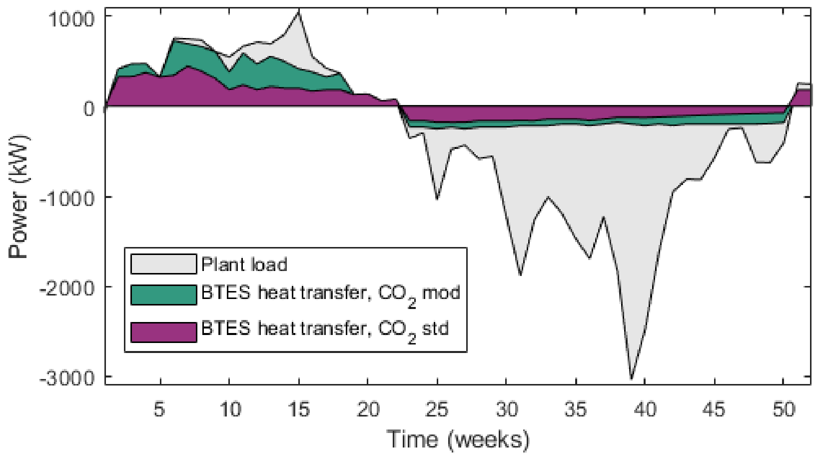

Figure 20: BTES heat transfer, in-parallel configuration, optimized operation. Positive power corresponds to BTES charging, negative to discharging.

The calculated reduction of CO_2 emissions using the three optimal control approaches under the two considered CO_2 intensity profiles is reported in Table 7.

Table 7: Yearly CO_2 emissions and reduction relative to the portion of heating and cooling covered by the BTES in each optimal control case and CO_2 intensity profile scenario.

	Base emissions (t_{CO_2}/y)	Opt. ctrl. emissions (t_{CO_2}/y)	CO_2 difference
Opt Ser (std)	38.5	33.1	-13.9%
Opt Par (std)	45.9	40.1	-12.8%
Opt Mix (std)	43.5	37.2	-14.5%
Opt Ser (mod)	44.6	35.7	-19.9%
Opt Par (mod)	60.5	49.4	-18.4%
Opt Mix (mod)	59.4	47.9	-19.2%

As it can be noticed from this table, the effective reduction of CO_2 emissions of the BTES is in the order of 13-14% in the standard CO_2 intensity profile scenario, and in the order of 18-20% in the modified CO_2 intensity profile scenario, hinting that with a more balanced heating and cooling demand and with better sized BTES, larger CO_2 reductions are possible. When considering these results, it should be noted that the potential presence of ground water flow, detrimental to the efficiency of the storage, was not modelled.

As these results highlight that the demand boundary conditions, system design and BTES sizing are crucial in achieving a significant reduction at system-level, the following section presents a methodology to formulate an optimization problem that encompasses simultaneously the design and operation problems, simplifying the detail of the latter but retaining the key principles found important in this control study.

3. BTES design optimization

This second part of the study considers a generic district heating and cooling system configuration with centralized energy generation and storage. Seasonal thermal energy storage is achieved via a cylindrical BTES with an in-parallel plumbing configuration. In line with the requirement of avoiding the use of fossil fuels for heat generation, electricity is assumed to be the only primary source of energy for the provision of on-demand heating and cooling. Therefore, it is assumed that the buildings' cooling demand can be met by two chillers, one that rejects the waste heat in a BTES and a second one that uses the ambient air as a sink. The heating demand can be met by two heat pumps, also using the BTES and the ambient air as sources.

As the total heating demand of the site might differ significantly from the cooling one, an additional solar thermal heat source can be considered in the design optimization of the system. The solar thermal system is assumed to be able to provide heat either directly to the district heating system, or store it into the BTES. It is assumed that the solar thermal collectors are coupled with a buffer tank large enough to absorb daily fluctuations in energy generation.

Figure 21 shows the described setup the operated in cooling mode and BTES charging, as well as in heating mode and BTES discharging.

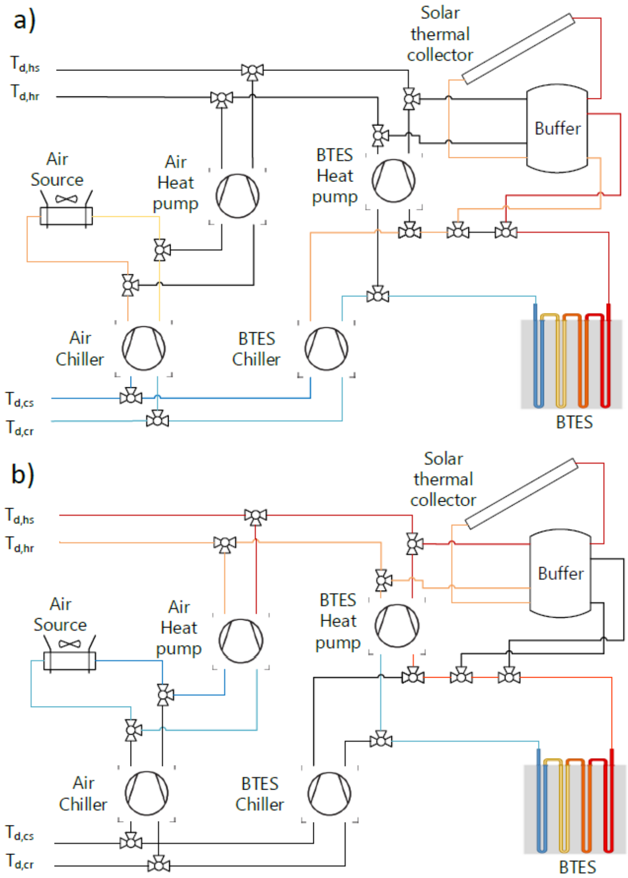

Figure 21: Case study operating in a) cooling mode and BTES charging, and in b) heating mode and BTES discharging.

The design optimization of the energy system considered in this study has the objective of fulfilling the thermal energy demand of the district, while minimizing the yearly cost of the energy system. This cost comprises of capital and operational components, with an additional operational cost associated with the CO_2 emissions of the system. The CO_2 emissions price is used in this study as a key decision variable to influence the system design and configuration.

3.1 Design optimization framework

The optimization framework is designed to take as input data the weather conditions (solar radiation I_t and ambient temperature T_a), CO_2 intensity profile (I_{CO2}), and heating and cooling demand profiles $P_{load,heat}$ and $P_{load,cool}$) are the primary sets of inputs to the optimization problem, which returns the optimal system design in terms of technology sizing and operational conditions. The input weather, CO_2 intensity and demand data are provided for a year with an hourly resolution, and they are assumed not to change along the lifetime of the system.

The optimization returns, under defined boundary conditions, the best sizing and operational decision variables for the energy system considered, assuming that the defined heating and cooling demand must be met. These decision variables include:

- The optimal equipment sizing, including the heat pump and chillers thermal capacity (S_{hp_BT},S_{ch_BT},S_{hp_a},S_{ch_a}), solar thermal collectors area (S_{sol}), and volume of the BTES (discretized, V_j).
- The optimal temperature difference between fluid and BTES in charging with the chiller and discharging with the heat pump (ΔT_{ch} and ΔT_{hp} respectively) and optimal initial temperature of the BTES temperature swing $T_{BT,init}$).
- The fraction of heating and cooling demand provided, at each time step k, by the solar generation (P_{th,sol_used}), by the heat pump and chiller connected to the BTES (P_{th,hp_BT}, P_{th,ch_BT}) or by the air-source heat pump and chiller (P_{th,hp_a}, P_{th,ch_a}).
- The fraction of solar generation, at each time step, stored in the BTES (P_{th,sol_tr}).

The electrical power consumption of the energy system ($P_{el,tot}$) at each time step is calculated, as the sum of the contribution from all the heat pumps and chillers considered, to estimate the operational costs and CO_2 emissions to be included in the optimization objective function. The electrical power consumption of circulation pumps is not considered in this study, as if the piping is well designed, this consumption is significantly smaller than the heat transferred, as reported in [25].

For this optimization problem, the BTES sizing was discretized as the properties of the storage change with the storage volume, such as the thermal losses and the possibility to transfer heat.

The BTES is assumed to be cylindrical, with uniformly distributed boreholes, and employing an in-parallel plumbing configuration such that it can be modelled as a single capacitance with losses calculated with the steady-state equation proposed in [34]. The heat losses occur through the insulation, which has an area equal to A_i and a U-value U_i, through the uninsulated part of the BTES. These losses are expressed as a function of the storage depth, storage aspect ratio and ground thermal conductivity. The set of storage sizes contains n_j elements, each corresponding to a storage volume V_j.

To linearly model the relation between the maximum heat transfer rate and the temperature difference between the ground and the heat transfer fluid, an equivalent UA_j coefficient is calculated for each BTES configuration, which assumes the ground heat exchangers at a constant borehole wall temperature equal to the overall BTES temperature. This UA coefficient was identified as presented in Section 2 and in [25].

As it is assumed that the storage keeps the same aspect ratio (diameter equal to depth) when scaled, the heat loss factor h for the proposed steady-state heat loss formulation is the same in each of the various sizes considered.

The BTES cost (J_{BT}) in each scaling option is obtained from the total drilling length, calculated as the product of the number of ground heat exchangers and their depth, multiplied by a drilling price per meter (λ_{GHX}) and an annuity factor (ω_{BT}).

Furthermore, the heat transfer is constrained in each storage configuration by the total UA value (UA_j) of the ground heat exchangers and temperature difference between heat transfer fluid and storage (ΔT_{ch}, ΔT_{hp},T_{sol} - T_{BT}). The storage temperature evolution and constraints in each configuration j are presented in Eq. 3:

$$\begin{cases} T_{BT}(k+1) & = T_{BT}(k) + \frac{\Delta t}{M_g V_j}(P_{th,ch\_BT}(k) - P_{th,hp\_BT}(k) + \\ & \quad P_{th,sol\_tr}(k) - U_i A_{i,j}(T_{BT}(k) - T_a(k)) - k_g h \frac{D_j}{2}(T_{BT}(k) - T_g)) \\ P_{th,ch\_BT}(k) <= UA_j \Delta T_{ch} \\ P_{th,hp\_BT}(k) <= UA_j \Delta T_{hp} \\ P_{sol,tr}(k) <= UA_j(T_{sol} - T_{BT}(k)) \\ J_{BT} = D_j n_{GHX,j} \lambda_{GHX} \omega_{BT} \end{cases} \tag{3}$$

where T_{BT} is the temperature of the storage, T_a the ambient temperature, T_{sol} the supply temperature of the solar system and T_g the undisturbed ground temperature.

A number of constraints are also introduced in the optimization problem, to ensure that i) only one size of storage can be selected at a time, ii) that the storage temperature stays within predefined boundaries, iii) that the storage temperature (and therefore energy content) are the same at the beginning and end of the year.

Similar constraints are placed on the rest of the equipment of the energy system, ensuring that for example, the thermal output at each time step of each heat pump or chiller does not exceed their capacity. Furthermore, as in the operation optimization study presented in Section 2, the inverse of the COP of this equipment is linearized in the relevant operating range to enable numerical optimization methods to be applied.

Lastly, the heating and cooling demand must be met by the system with the available heat pumps, chillers and solar resources.

The objective function of the optimization problem represents the total annual cost of the energy system J, which includes a capital component (J_c), and operational components related to energy consumption ($J_{o,e}$) and CO_2 emissions ($J_{o,CO2}$).

The annual capital cost is expressed as the sum of the equipment cost (Eq. 4):

$$J_c = \omega_{eq}(\lambda_{hp}(S_{hp\_BT}+S_{hp\_a})+\lambda_{ch}(S_{ch\_BT}+S_{ch\_a})+\lambda_{sol}S_{sol}+\lambda_{ST}S_{ST})+J_{BT} \quad (4)$$

where each λ is the equipment price (i.e. capital cost per unit of size for each of the considered equipment) and ω is the annuity factor. For simplicity and ease in interpreting the results, interest rates and respective discounting were not considered in this study.

Assuming ν_{el} as a constant electricity price per kWh, the operational cost related to the energy consumption $J_{o,e}$ is calculated as in Eq. 5.

$$J_{o,e} = \sum_{k=1}^{N}(P_{el,tot}(k))\nu_{el}\Delta t \quad (5)$$

Similarly, integrating the product of electricity consumption and CO_2 intensity at each time step k and considering a constant CO_2 price, the total CO_2 emissions operational cost $J_{o,CO2}$ is calculated as in Eq. 6.

$$J_{o,CO_2} = \sum_{k=1}^{N}(I_{CO2}(k)P_{el,tot}(k))\nu_{CO_2}\Delta t \quad (6)$$

3.2 Design study implementation

The input heating and cooling demand data used in this study were the same as the one presented in Section 2, but at a higher temporal resolution (averaged daily). The employed Dübendorf TMYx weather data was sourced from [35]. Different sizes are considered with the same cylindrical shape and aspect ratio. In particular, the BTES depth and diameter are assumed to be equal, to minimize its thermal losses. Therefore the heat loss shape coefficient h was assumed to be equal to 21.2, as suggested in [34]. The thermal conductivity of the BTES top insulation U_i was assumed to be equal to 0.14 W/m.K. As the ground heat exchangers are assumed to be uniformly distributed, a BTES increase in size implies the installation of more and deeper boreholes. The length and number of boreholes are thus changed according to the total volume of the BTES storage. Five BTES configurations were considered by the optimization framework, in addition to the case without a BTES. The annual cost of the BTES was calculated assuming a lifetime of 60 years, with the construction characteristics presented in Table 8. The BTES cost was calculated from a ground heat exchanger cost of installation per meter equal to 66€/m [36]. The undisturbed ground temperature was assumed to be equal to 12°C, and the minimum operating temperatures of the storage were set at 6°C and 65°C respectively. The initial temperature range of the BTES was constrained between 8°C and 30°C, as typical heat pump-driven BTES systems in balanced operation would have a lower operation boundary in a similar range, as reported in [37].

Table 8: BTES discrete sizing options considered by the optimization.

Bool var.	Diam./Depth (m)	Volume ($\times 10^3 m^3$)	UA (kW/K)	n_{GHX}
$\delta(1)$	53.4	119.2	22.5	158
$\delta(2)$	61.2	179.6	33.8	207
$\delta(3)$	70.0	269.4	50.6	271
$\delta(4)$	80.1	404.1	76.0	355
$\delta(5)$	91.7	606.1	113.9	466
$\delta(6)$	0	0	0	0

The parameters and prices of the heat pumps, chillers and solar collectors are summarized in Table 9. For this equipment, a lifetime of 20 years was assumed.

Table 9: Heat pumps, chillers and solar thermal collectors price and maximum size.

Parameter	λ	S^{max}
S_{sol}	500 €/m²	10^4 m²
S_{hp_BT}, S_{hp_a}	576 €/kW	3307.4 kW
S_{ch_BT}, S_{ch_a}	576 €/kW	974.5 kW

The efficiency of the collectors η_{sol} was assumed to be equal to 0.65. The short-term storage volume which is assumed to be proportional to the collector area was assumed to have a cost (λ_{ST}) equal to 9€/kWh [38].

As only operational CO_2 emissions are considered in this study, no emissions are associated with the heat generation of the solar thermal collectors. The electricity price ν_{el} was assumed to be constant at 0.156€/kWh [39]. A range of CO_2 prices from 50€/t to 500€/t was tested. As a reference, the lower limit is approximately the current EU carbon price [40], while direct extraction of CO_2 from the atmosphere is estimated to cost between 110€/t and 280€/t [41].

3.2.1 Testing procedure

To evaluate the effect on the optimal design and operation of the energy system of boundary conditions such as the ratio of cooling demand in relation to the heating one, and the seasonal variation in CO_2 intensity of the electricity used, four testing scenarios were considered. Considering the heating and cooling demand ratio, the following scenarios were considered:

- standard cooling demand profile, as presented in Section 2.
- increased cooling demand profile, where the cooling is three times larger than in the standard scenario, and therefore of approximately the same order of magnitude as the heating demand.

The current Swiss seasonal CO_2 intensity profile follows a sinusoidal trend [33], with lower intensity in summer compared to the one in winter. To represent the current and a higher penetration of renewable energy in the summer electricity generation, the same standard and modified CO_2 intensity profile presented in Figure 16 were used.

The optimization was performed in each scenario considering different CO_2 prices in the aforementioned range, to assign more or less priority to the CO_2 emissions. The results from this set of optimizations were replicated with and without the possibility to include solar thermal collectors to support the energy system.

3.3 Design optimization results

In this section, the results from the application of this methodology to the selected case described are presented. First, the results from the system design optimization without the possibility to integrate solar generation are described, to highlight the effect of the boundary conditions specifically on the BTES design and its operation. In a second subsection, the results from the same optimization, including the possibility to include solar thermal collectors, are shown.

3.3.1 Results without solar integration

The results from the BTES optimization without an additional solar heat source show that in the standard cooling demand scenario, seasonal storage is useful, but with a limited volume, as shown in Figure 22a. This is mostly because the cooling and the heating demand are unbalanced in this case, and only a portion of the latter can be covered using the BTES as the rejected heat from cooling operations is limited. It is noticeable from the operational results in the same figure that the increase in CO_2 emissions price has the effect of increasing the initial storage temperature, as well as a slightly higher temperature difference in charging (ΔT_{ch}) to enable a higher heat transfer rate to the storage. This results in a generally higher operating temperature of the BTES. This behaviour is even more evident in the modified CO_2 intensity profile scenario, as the benefits from gaining efficiency in winter, even if some is lost in summer, are even more pronounced.

Observing the optimization results in Figure 22b, which presents the scenario with increased cooling demand, it can be seen that the optimal BTES size is the largest in almost all CO_2 emissions prices, in both CO_2 emissions profile scenarios considered.

In this increased cooling demand scenario, the optimal BTES initial temperature increases with the CO_2 emissions price even more than in the standard cooling demand scenario, particularly with the modified CO_2 emissions profile as a boundary condition.

This increase in operating temperature, while being beneficial to the discharging COP of the heat pump, leads to a lower efficiency of the BTES. As the operating temperature is fluctuating around the undisturbed ground temperature when the CO_2 emissions price is the lowest, the thermal losses are expected to be minimal. With higher CO_2 price, the storage efficiency decreases but remains around 80%.

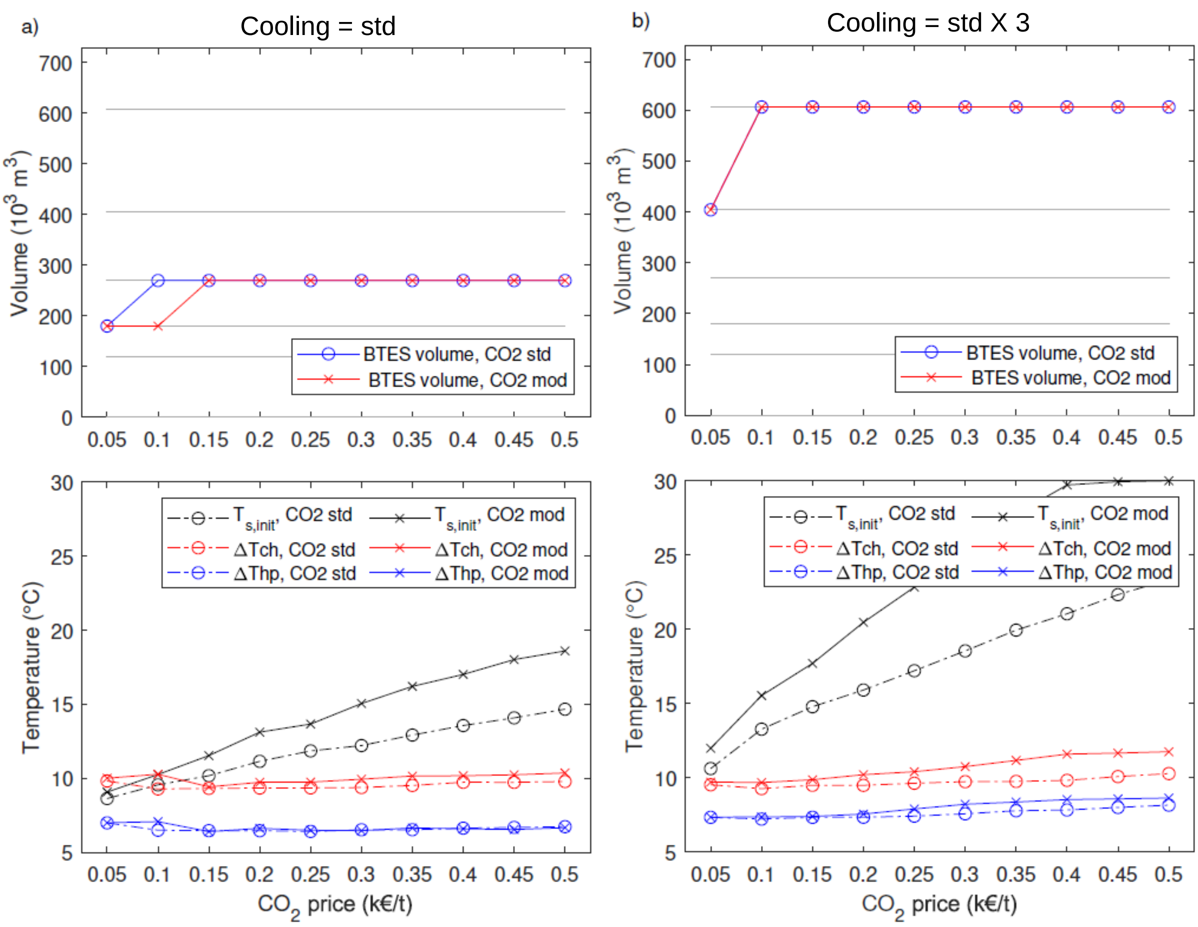

Figure 22: Optimal BTES size (top) and operation (bottom) as a function of the CO_2 cost, in the a) standard cooling demand and b) increase cooling demand (3X) scenarios.

The optimal system design solutions, as shown in Figure 23, form different Pareto fronts depending on the scenario. The scenarios with the standard cooling profile (black lines) present a relatively narrow range for system optimization possibilities to reduce emissions. Compared to a base system without BTES, in the case of the standard CO_2 profile, this emissions reduction ranges from 4.1 to 6.7%.

The modified CO_2 profile enables a slightly larger emissions reduction opportunity, from 3.9% to 8.1%. This is achieved with a yearly cost (excluding the CO_2 emissions cost), ranging from 0.3% lower to 0.3% higher.

The scenario with the increased cooling demand profile (red lines) offers a significantly larger emissions reduction opportunity which, in the best case (modified CO_2 profile), ranges from 9.8% to 27.1%, with an annual cost from 0.6% lower to 1.5% higher than the system without a BTES.

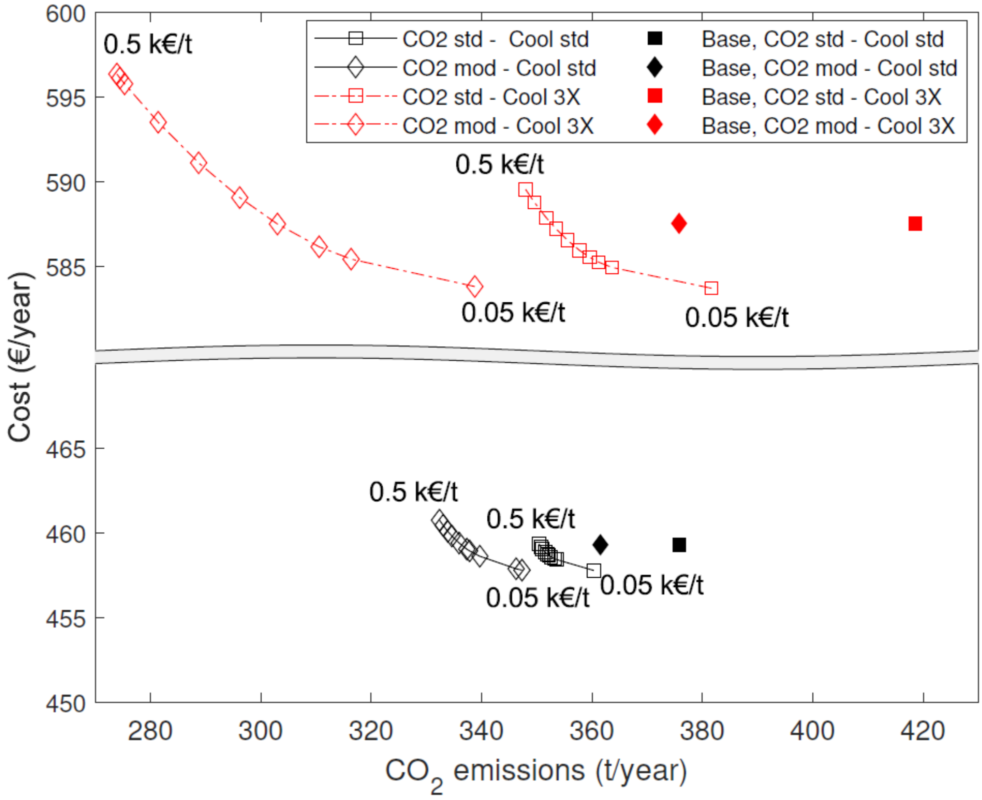

Figure 23: Optimal system solutions under the different CO_2 intensity profile (square and rhomboidal markers) and cooling demand scenarios (black and red lines), without integration of solar generation. The "base" setup, without a BTES, is presented with a filled marker for each scenario.

3.3.2 Results with solar integration

In this second optimization result set, in addition to the BTES, the possibility to install a solar thermal array to support the energy system was also considered. As it can be observed from the sizing and operational results in Figure 24, the solutions found for the standard cooling demand profile (Figure 24a) and the increased one (Figure 24b) show that above a defined carbon price (0.1k€/t and 0.15k€/t respectively) including a solar thermal source becomes economical advantageous as an addition to the waste heat recovered from the cooling operations. In both figures it is noticeable that, once it becomes feasible, the optimal size of the collector array increases as expected with the CO_2 price, and the heat pump size slightly decreases as some of the heating demand can be met directly by the solar generation.

As expected, in the standard cooling demand profile scenario (Figure 24a) the optimal size of the solar collectors' array is larger than the one calculated in the increased cooling demand profile scenario (Figure 24b), but with a relatively smaller supporting BTES.

The CO_2 intensity profile has also an impact on the optimal sizing of the solar array. A modified CO_2 intensity profile favours the rejection of heat of cooling operations leads to smaller optimal solar array sizes for the same CO_2 price.

At the same time, above the 0.1k€/t and 0.15k€/t thresholds, the operation of the BTES changes from low to high-temperature, as more heat becomes available from solar collectors in summer at elevated temperatures and without direct CO_2 emissions. This can be seen from the initial storage temperature in the bottom graphs (black lines) of Figure 24a and Figure Figure 24b.

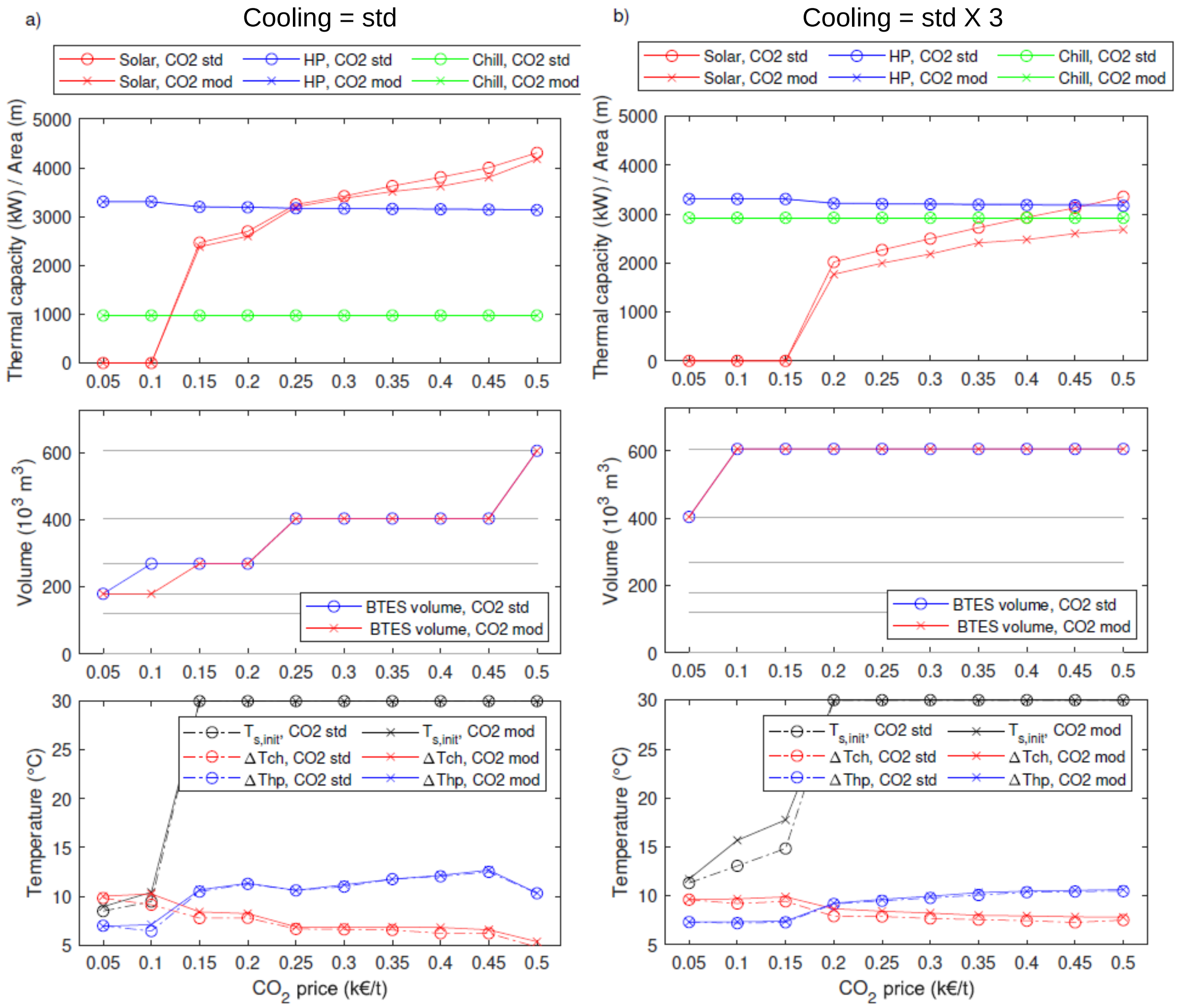

Figure 24: Optimal solar, heat pump and chiller size (top), BTES size (top) and operation (bottom) as a function of the CO_2 price, in the a) standard cooling demand and b) increase cooling demand (3X) scenarios.

As shown in Figure 25, the possibility to include solar thermal generation enables a wider yearly CO_2 reduction range, even in the standard cooling demand scenarios. In the standard cooling scenario, the reduction ranged from 3.9-4.1% with the lowest CO_2 price to 41.3-43.7% with the highest one.

This was achieved with an annual cost ranging from 0.3% lower to 5.9-6.1% higher. In the increased cooling demand scenario the calculated reduction ranged from 9.0-9.7% with the lowest CO_2 price to 34.8-38.6% with the highest one, achieved with an annual cost ranging from 0.6% lower to 2.3-3.1% higher. As expected, the integration of a solar thermal array provides better system solutions at CO_2 prices higher than 0.10-0.15k€/t, enabling a higher CO_2 reduction for the same annual cost as the case without solar.

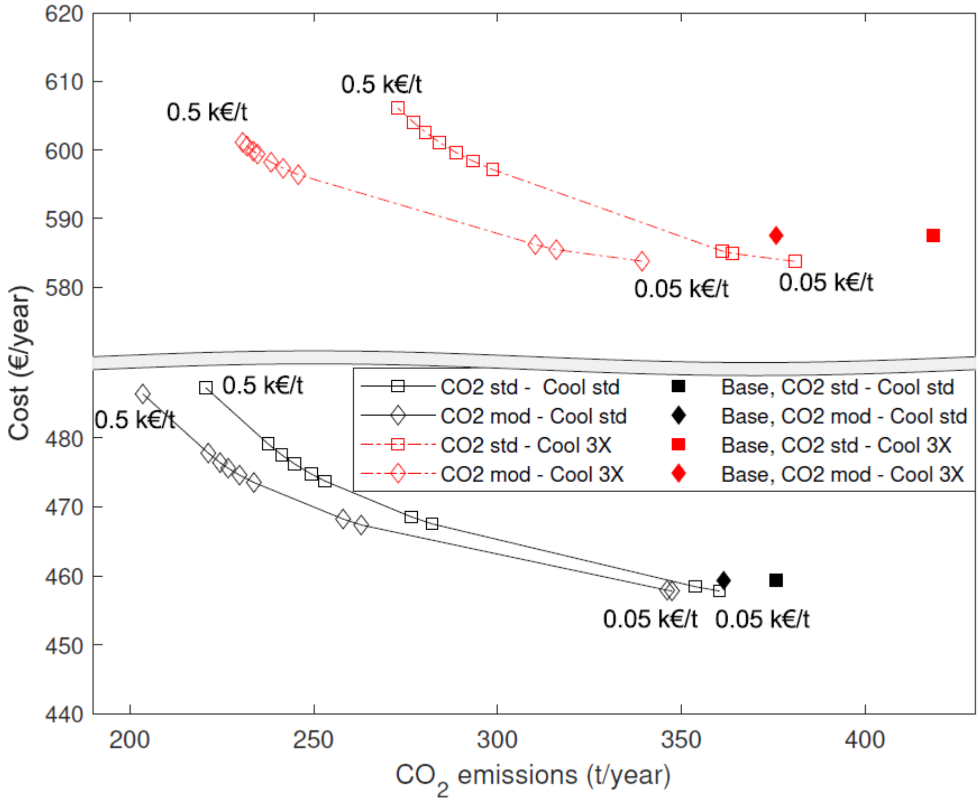

Figure 25: Optimal system solutions under the different CO_2 intensity profile (square and rhomboidal markers) and cooling demand scenarios (black and red lines), with the integration of solar generation. The "base" setup, without a BTES or solar collectors, is presented with a filled marker for each scenario.

4. Conclusions and Recommendations

While current trends are going towards district energy systems and seasonal thermal energy storages at lower temperatures, the hypothesis that was to be tested in this study is that the operating conditions of such system and storage, in particular operating temperatures, are a critical factor in determining system's performance under defined boundary conditions.

In this study the problem was approached by developing a replicable design and operation optimization methodology for energy systems with a BTES, modelling the dynamics of a BTES system in a numerically tractable way to enable optimization algorithms to find the best system configuration while retaining the key physical phenomena that guarantee a good prediction performance.

The first part of the study focused on finding the best operating conditions of a defined BTES and district heating and cooling system. A modelling method, based on a resistance–capacitance (R–C) equivalence and linearized heat transfer calculation within the boreholes, was successfully developed and calibrated against a high-fidelity TRNSYS model. This model was then utilized to optimize the performance of a BTES system based on a case study, aiming at minimizing CO_2 emissions.

Applying the optimization to the same system under two different boundary conditions, a standard one and a second one with reduced intensity during cooling dominated periods, it was evident that under the standard intensity profile conditions a lower temperature BTES would perform better, while in the modified emission intensity profile scenario, the optimal operation of the BTES would require a higher supply and discharge temperature, resulting in higher temperature swing.

The results showed that the optimal controllers could take advantage of the BTES and changes in seasonal CO_2 intensity to reduce the yearly CO_2 emissions of the system by 2.2% with the standard CO_2 intensity profile and by 4.3% with the modified one. The limited reduction is attributable to the fact that the cooling and heating demands of the case study are not balanced, with a heating demand being significantly larger than the cooling one, and the storage being small in comparison to the demand. Nevertheless, considering only the emissions associated with the heating and cooling provided via the BTES in the various optimal control scenario and comparing them with the emissions from the base system, a reduction in the range of 13%–20% was calculated.

Extending the study to the optimization of the design of the components of the energy system, while still considering key operational parameters, proved to enable finding interesting additional interesting results. The primary objective of this second optimization was reducing the total system CO_2 emissions and its total cost. Varying prices associated with the carbon emissions were used to assign a higher or lower priority to the CO_2 emissions component. Results show that, when only considering the waste heat from cooling operations as a source of heat for the BTES, increasing the price of the CO_2 emissions would not only increase the optimal size of the BTES, but as expected from the results from the first study, also its operating temperature, to take advantage of the seasonal variation in the CO_2 intensity profile. When the possibility to integrate solar thermal collectors as an additional heat source was considered, the optimal size of the BTES increased with the CO_2 price also in this case, together with the size of the solar array as soon as the integration of solar collectors became economically viable (above a CO_2 price of 0.1-0.15k€/t). At the same time, the optimal operation of the BTES changed, working at a higher temperature as soon as the solar generation was introduced in the system design.

While the opportunity of reducing the CO_2 emissions, compared to a baseline system without a BTES, was quite limited in the case of a system without solar collectors and with standard cooling demand and CO_2 intensity profile (from 4.1% with the lowest CO_2 cost, up to 6.7% with the highest), an increase in cooling demand and modification of the CO_2 prole would improve the potential reduction up to 27.1%.Including the possibility to integrate a solar thermal array enables the system design to further expand the potential CO_2 emissions reduction, up to 34-43% in the best-case scenarios. All these reductions were achieved with a comparably small increase in annual cost, up to 6.1%, highlighting that seasonal thermal energy storage could help access untapped CO_2 reduction potential at a reasonable cost, or legislative interventions such as a moderate CO_2 tax could make them one of the preferred technological solutions.

National and International Collaboration

This research in the domain of seasonal thermal energy storage (STES) connects well with other Empa lab internal activities on the level of neighbourhood and district energy systems. Furthermore, this work is strongly interfacing with the work of others in the domain of STES and thermal network-related research. Accordingly, this research activity is emphasized and extended in the frame of other longer-term research programmes (e.g. SWEET DeCarbCH, SWEET PATHFNDR, SNF Sinergia SOTES). International Collaboration is also sought for through European research projects (e.g. H2020 EcoCube) and further research proposals, such one for the current JPP-SES and ERA-Net Geothermica, where the experimental testing of the BTES currently being constructed for the energy system of the Empa campus is proposed. It is, therefore, envisioned that the methods developed in this project will serve as a basis for answering several other upcoming research questions in the field of optimal design and operation of STES.

Communication

Two research articles were prepared, one presenting modelling and operation optimization results (published in Applied Thermal Engineering [25]), and a second one, currently under review, presents the design optimization methodology and relative results [26].

Evaluation and Outlook

Beyond this project, the methodology proposed in this study could serve as a basis for further research projects in the field of optimal design and operation of energy systems integrating a BTES, aiming for example at extending the capabilities of the proposed framework to include the effect of networks and their operational conditions, the modelling of distributed or centralized setups, as well as the effects of interventions at building-level on the energy system design. Boundary conditions could also be integrated and assed differently, considering for example that they might evolve during the lifetime of the system (e.g. CO2 and electricity prices, climatic boundary conditions and energy demand) These efforts are also envisioned to support tools for an easier early-stage design of such energy system, helping a larger adoption of seasonal thermal energy storage technologies.

References

[1] Schmidt T, Alex P. Monitoring Results from Large Scale Heat storages for District Heating in Denmark 2018.

[2] Tordrup KW, Poulsen SE, Bjørn H. An improved method for upscaling borehole thermal energy storage using inverse finite element modelling. Renew Energy 2017;105:13–21. https://doi.org/10.1016/J.RENENE.2016.12.011.

[3] Gao L, Zhao J, Tang Z. A Review on Borehole Seasonal Solar Thermal Energy Storage. Energy Procedia 2015;70:209–18.

[4] Fisch M., Guigas M, Dalenbäck J. A REVIEW OF LARGE-SCALE SOLAR HEATING SYSTEMS IN EUROPE. Sol Energy 1998;63:355–66. https://doi.org/10.1016/S0038-092X(98)00103-0.

[5] Lundh M, Dalenbäck J-O. Swedish solar heated residential area with seasonal storage in rock: Initial evaluation. Renew Energy 2008;33:703–11. https://doi.org/10.1016/J.RENENE.2007.03.024.

[6] Heier J, Bales C, Sotnikov A, Ponomarova G. Evaluation of a high temperature solar thermal

seasonal borehole storage. 30th ISES Bienn Sol World Congr 2011, SWC 2011 2011;6:4709–18. https://doi.org/10.18086/swc.2011.29.10.

[7] Ruesch F, Gupta R Das, Haller M, SPF Institut für Solartechnik H für THSR. Hotspot - Speicherung solarer Wärme im Untergrund auf direkt nutzbarem Temperaturniveau - Anforderungen und mögliche Schweizer Standorte. Bundesamt für Energie BFE; 2018.

[8] Nussbicker J, Mangold D, Heidemann W, Muller-Stenhagen H. Solar Assisted District Heating System with Duct Heat Store in Neckarsulm-Amorbach (Germany). ISES Sol World Congr 2003 2003:1–6.

[9] Schmidt T, Mangold D, Müller-Steinhagen H. Central solar heating plants with seasonal storage in Germany. Sol Energy 2004;76:165–74. https://doi.org/10.1016/j.solener.2003.07.025.

[10] Bauer D, Marx R, Nußbicker-Lux J, Ochs F, Heidemann W, Müller-Steinhagen H. German central solar heating plants with seasonal heat storage. Sol Energy 2010;84:612–23. https://doi.org/http://dx.doi.org/10.1016/j.solener.2009.05.013.

[11] Reuss M, Beuth W, Schmidt M, Schoelkopf W. Solar district heating with seasonal storage in Attenkirchen. Proc IEA Conf ECOSTOCK, Richard Stock Coll Pomona, New Jersey, USA 2006.

[12] Lanahan M, Tabares-Velasco P. Seasonal thermal-energy storage: a critical review on BTES systems, modeling, and system design for higher system efficiency. Energies 2017;10:743.

[13] Sibbitt B, McClenahan D, Djebbar R, Thornton J, Wong B, Carriere J, et al. The Performance of a High Solar Fraction Seasonal Storage District Heating System – Five Years of Operation. Energy Procedia 2012;30:856–65. https://doi.org/10.1016/J.EGYPRO.2012.11.097.

[14] Zhang R, Lu N, Wu YS, The Geo-Institute of the American Society of Civil E. Efficiency of a community-scale borehole thermal energy storage technique for solar thermal energy. GeoCongress 2012 State Art Pract. Geotech. Eng. 225 GSP, Oakland, CA: 2012, p. 4386–95. https://doi.org/10.1061/9780784412121.451.

[15] Mcdowell T, Thornton J. SIMULATION AND MODEL CALIBRATION OF A LARGE-SCALE SOLAR SEASONAL STORAGE SYSTEM, 2008.

[16] Nilsson E, Rohdin P. Performance evaluation of an industrial borehole thermal energy storage (BTES) project – Experiences from the first seven years of operation. Renew Energy 2019;143:1022–34. https://doi.org/https://doi.org/10.1016/j.renene.2019.05.020.

[17] Guo F, Zhu X, Zhang J, Yang X. Large-scale living laboratory of seasonal borehole thermal energy storage system for urban district heating. Appl Energy 2020;264:114763. https://doi.org/10.1016/J.APENERGY.2020.114763.

[18] Buffa S, Cozzini M, D'Antoni M, Baratieri M, Fedrizzi R. 5th generation district heating and cooling systems: A review of existing cases in Europe. Renew Sustain Energy Rev 2019;104:504–22. https://doi.org/https://doi.org/10.1016/j.rser.2018.12.059.

[19] Amstein+Walthert. Richti wallisellen. 2000.

[20] Sulzer M, Summermatter S, Hochschule Luzern HSLU Lauber Iwisa AG EAG. Solare Energieversorgung im alpinen Raum - Reka-Feriendorf Blatten-Belalp. Bundesamt für Energie BFE; 2016.

[21] Energieschweiz. Fallbeispiele „ Thermische Netze “. 2019.

[22] Vetterli N, Sulzer M, Menti UP. Energy monitoring of a low temperature heating and cooling district network. Energy Procedia 2017;122:62–7. https://doi.org/10.1016/j.egypro.2017.07.289.

[23] EnergiAlpina. Prinzipschema + Hybridanlage. n.d.

[24] Persson T, Stavset O, Ramstad RK, Alonso MJ, Lorenz K. Software for modelling and simulation of ground source heating and cooling systems. 2016.

[25] Fiorentini M, Baldini L. Control-oriented modelling and operational optimization of a borehole thermal energy storage. Appl Therm Eng 2021:117518. https://doi.org/10.1016/J.APPLTHERMALENG.2021.117518.

[26] Fiorentini M, Heer P, Baldini L. Design optimization of a borehole seasonal thermal energy storage in a district heating and cooling system. Energy n.d.

[27] Pahud D, Fromentin A, Hadorn JC. The Superposition Borehole Model for TRNSYS (TRNSBM). User Manuel, Internal Report, LASEN-EPFL, Lausanne; 1996.

[28] Eskilson P, Claesson J. Simulation model for thermally interacting heat extraction boreholes. Numer Heat Transf 1988;13:149–65. https://doi.org/10.1080/10407788808913609.

[29] Weber R, Baldini L. High Temperature Seasonal BTES for Effective Load Shifting and CO2 Emission Reduction. Eurosun 2018 – 12th Int. Conf. Sol. Energy Build. Ind., Rapperswil, Switzerland: 2018, p. 1–9. https://doi.org/10.18086/eurosun2018.13.04.

[30] Bauer D, Heidemann W, Müller-Steinhagen H, Diersch H-JG. Thermal resistance and capacity models for borehole heat exchangers. Int J Energy Res 2011;35:312–20. https://doi.org/https://doi.org/10.1002/er.1689.

[31] Lofberg J. YALMIP : a toolbox for modeling and optimization in MATLAB. 2004 IEEE Int. Conf. Robot. Autom. (IEEE Cat. No.04CH37508), 2004, p. 284–9. https://doi.org/10.1109/CACSD.2004.1393890.

[32] Gurobi. Gurobi Solver n.d. https://www.gurobi.com/products/gurobi-optimizer/ (accessed November 10, 2020).

[33] electricitymap n.d. https://www.electricitymap.org/map (accessed November 2, 2020).

[34] Hellström G. Ground heat storage: Thermal analyses of duct storage systems. Lund Univ 1991:310.

[35] Lawrie L, Drury C. Development of Global Typical Meteorological Years (TMYx) 2019. http://climate.onebuilding.org (accessed June 3, 2021).

[36] Luo J, Rohn J, Bayer M, Priess A. Thermal performance and economic evaluation of double U-tube borehole heat exchanger with three different borehole diameters. Energy Build 2013;67:217–24. https://doi.org/10.1016/j.enbuild.2013.08.030.

[37] Skarphagen H, Banks D, Frengstad BS, Gether H. Design Considerations for Borehole Thermal Energy Storage (BTES): A Review with Emphasis on Convective Heat Transfer. Geofluids 2019;2019. https://doi.org/10.1155/2019/4961781.

[38] Petkov I, Gabrielli P. Power-to-hydrogen as seasonal energy storage: an uncertainty analysis for optimal design of low-carbon multi-energy systems. Appl Energy 2020;274:115197. https://doi.org/10.1016/j.apenergy.2020.115197.

[39] ElCom electricity tariffs n.d. https://www.strompreis.elcom.admin.ch (accessed April 30, 2021).

[40] EMBER Daily EU ETS carbon price n.d. https://ember-climate.org/data/carbon-price-viewer/ (accessed April 30, 2021).

[41] IEA. Levelised cost of CO2 capture by sector and initial CO2 concentration 2019. https://www.iea.org/data-and-statistics/charts/levelised-cost-of-co2-capture-by-sector-and-initial-co2-concentration-2019.